TephAta - An online collection of tephra data from the Atacama Desert

Niklas Leicher[1], Vincent Feldmar[2], Andrés Quezada Jara[3], Paulina Vásquez Illanes[3], Fernando Sepúlveda Vásquez[3], Frank Wombacher[1], Markus Lagos[4], Tanja Kramm[2], Gabriel González[5], Klaudia Kuiper[6], Christoph Breitkreuz[7], Alberto Sáez[8], Domingo Gimeno[9], Lluís Cabrera[8], Inés Rodríguez Araneda [10], Bernd Wagner[1], Georg Bareth[2], Volker Wennrich [1]

[1]Institute of Geology and Mineralogy, University of Cologne, Cologne, 50672, Germany
[2]Institute of Geography, University of Cologne, Cologne, 50672, Germany
[3]Servicio Nacional de Geología y Minería (SERNAGEOMIN), Avenida Santa María 0104, Providencia, Santiago, Chile
[4]Institute of Geosciences and Meteorology, University of Bonn, Bonn, 53115, Germany
[5]National Research Center for Integrated Natural Disaster Management, Departamento de Ciencias Geológicas, Universidad Católica del Norte, Antofagasta, Chile
[6]Department of Earth Sciences, Vrije Universiteit Amsterdam, Amsterdam, Netherlands
[7]Institut für Geologie und Paläontologie, Bernhard-von-Cotta-Str. 2, TU Bergakademie Freiberg, 09599 Freiberg, Germany
[8]Geomodels Research Institute, Department Dinàmica de la Terra i de l'Oceà, Universitat de Barcelona, Marti Franques s/n, 08028 Barcelona, Spain
[9]Department de Mineralogia, Petrologia i Geologia Aplicada, Universitat de Barcelona, 08028 Barcelona, Spain
[10]Departamento de Obras Civiles y Geología, Universidad Católica de Temuco, Temuco, Chile

Correspondence to: Niklas Leicher (n.leicher@uni-koeln.de)

Abstract

Tephrostratigraphy and tephrochronology are powerful tools using volcanic ash (tephra) layers for establishing stratigraphic correlations and/or to obtain chronological information for different kinds of sedimentary archives. To develop robust tephrostratigraphic frameworks it is essential to precisely characterize the physical, geochemical and chronological properties of tephra layers and their sampling sites. These frameworks allow newly discovered tephra layers to be correlated with established sequences, providing stratigraphic and chronological context and enhancing reconstructions of the spatial and temporal patterns of regional volcanic activity. Tephrostratigraphic frameworks have been developed or are currently emerging in many regions of the world. However, for some regions their potential remains underutilized. One such region is the Atacama Desert of northern Chile, despite its long history of frequent volcanism and associated tephra deposition. Within the framework of the Collaborative Research Centre "Earth – Evolution at the Dry Limit" (CRC1211), the glass phase geochemical compositions of Pleistocene tephra layers were recently systematically investigated to refine their stratigraphic and chronological placement. Alongside this effort, a dedicated tephra database, TephAta, was created to provide a long-term repository for tephrochronological research in the Atacama Desert. TephAta enables the comprehensive digital documentation of diverse tephra-related datasets within a single platform and offers search functionalities that support and streamline ongoing expansion of the regional framework, following FAIR (findability, accessibility, interoperability, and reusability) data principles. A first data release contains 106 tephra samples from 91 deposits, with continued spatial and temporal growth planned. All data are accessible via the TephAta portal (https://www.crc1211db.uni-koeln.de/tephata/, last access: 16 March 2026) and datasets described in this paper are available at https://doi.org/10.60520/IEDA/114209 (Leicher N., 2026). Beyond serving as a stratigraphic and chronological tool for paleoenvironmental or mapping studies, TephAta also facilitates investigations into the regions explosive volcanic history and supports volcanic hazard and risk assessment.

1 Introduction

Volcanic ash deposits are intercalated within many types of sedimentary sequences. This makes them highly valuable as isochronous marker horizons for stratigraphic and chronological studies in both geoscience and archaeology (Lowe, 2011). The geochemical composition of volcanic glass is one of the most commonly used and reliable parameters (Lowe et al., 2017) for correlating tephra layers and establishing tephrostratigraphic frameworks. During ash dispersal, aeolian fractionation often results in volcanic glass persisting as the dominant eruptive component with its relative abundance increases with distance from source. Owing to its quenched nature, the glass retains a geochemical composition that closely reflects the composition of the magma at the time of eruption, providing a distinctive fingerprint.

Tephrochronology is a well-developed and frequently used technique in many regions of the world including the Mediterranean (e.g., Sulpizio et al., 2003; Wulf et al., 2004; Giaccio et al., 2019; Leicher et al., 2021; Vakhrameeva et al., 2021), Northern Europe and the N-Atlantic (e.g., Griggs et al., 2014; Lowe et al., 2015; Abbott et al., 2018; Sáez et al., 2025), Central America (e.g., Kutterolf et al., 2016; Schindlbeck et al., 2018), New Zealand (e.g., Gehrels et al., 2006; Lowe et al., 2013; Hopkins et al., 2021) and eastern Asia (e.g., Sagawa et al., 2018; Albert et al., 2019; Portnyagin et al., 2020; Feng et al., 2022). Tephrochronological databases exist for specific regions, e.g., for (northern) Europe (TephraBase, Newton et al., 2007; Riede et al., 2011; RESET, Bronk Ramsey et al., 2015), the east African Rift (EarthD, Mana and Dimaggio, 2023), Alaska (GeoDIVA, Cameron et al., 2022), Kamchatka (TephraKam, Portnyagin et al., 2020), New Zealand (TephraNZ, Hopkins et al., 2021), southern Chile (BOOM!, Martínez Fontaine et al., 2023) or Antarctica (AnT, Kurbatov et al., 2014).

In some regions, however, tephrochronology remains underdeveloped, despite a long history of explosive volcanism that has produced frequent, widely dispersed tephra with diverse geochemical compositions. One such region is the western side of the Andes in Central South America, including the Atacama Desert. The Central Volcanic Zone of the Andes (14°-28° S; De Silva,

1989a) has a long volcanic eruptive history (c. 240 Ma; Oliveros et al., 2018) and is renowned for major explosive eruptive events during the Neogene (c. 25-1 Ma, cf. Wörner et al., 2000; Burns et al., 2015; Van Zalinge et al., 2016). Geochemical variations characteristic of individual volcanoes and eruptions are influenced not only by the composition of the parent magma and degree of crystallization, but also by the geodynamic evolution of the Andes. Spatial and temporal differences in the crustal thickness and composition have produced to varying degrees of magma-crust interactions, leading to diverse and often additional pathways of magmatic differentiation for individual eruptions (Kay et al., 2010; Brandmeier and Wörner, 2016; Burns and De Silva, 2023). The Atacama Deserts' long-term aridity is thought to have initiated as early as ca. 25 Ma ago (Dunai et al., 2005; Evenstar et al., 2017) and sets with the low degree of erosion and weathering (e.g., Ritter et al., 2023) suitable climatic conditions for the preservation of volcanic deposits. Despite dominating easterly wind systems, tephra deposits can be found abundantly from the Andes to the Pacific coast (Marquardt et al., 2005; Vásquez and Sepúlveda, 2013; e.g., Breitkreuz et al., 2014). Tephra layers serve as crucial isochronous markers for dating sedimentary sequences within these arid environments, where other dateable materials are scarce and the temporal resolution of sediment records is often low. Thus, tephra layers of the Atacama region hitherto were mainly directly dated to constrain paleoenvironmental and tectonic processes (Sáez et al., 2012; Kirk-Lawlor et al., 2013; Jordan et al., 2014) or for use in extended geological mapping of the Chilean National Geology and Mining Survey (SERNAGEOMIN; e.g., Medina et al., 2012; Blanco and Tomlinson, 2013; Sepúlveda et al., 2014; Vásquez et al., 2018). Correlation of tephra layers by their glass geochemistry to establish local stratigraphic correlations is rare in the Atacama Desert (Placzek et al., 2009; Breitkreuz et al., 2014; Tapia et al., 2015). In contrast, intensive research has been carried out on the magmatic evolution on the volcanoes of the Andes (e.g., De Silva, 1989b; Wörner et al., 2000; Kay et al., 2010; Mamani et al., 2010). Comprehensive results of this research including geochemical (whole-rock compositions and isotopes) and chronological data are made available within the Central Andes Geochemical and Geochronology database (https://andes.gzg.geo.uni-goettingen.de/). Whole-rock analyses, however, have been found to be less suitable for tephrochronological alignments due to site-dependent variations in their main components (variable relative abundances of glass, crystals and lithics) caused by aeolian fractionation, temporal eruptive variations and the influence of alteration (Tomlinson et al., 2012a; Lowe et al., 2017).Thus, a tephrostratigraphic framework based on glass geochemical compositions and geochronological data is currently missing at the western side of the Andes.

The Collaborative Research Centre "Earth – Evolution at the Dry Limit" (CRC1211) aims at disentangling how the shaping of land-surfaces by past episodes of wetter climate coevolved with the evolution of life in arid environments (Dunai et al., 2020). The main working area of the CRC is the Atacama Desert in Chile (Fig. 1a). For this multidisciplinary endeavor, establishing chronological control of the sedimentary climate archives and determining the timing and rates of surface processes are of fundamental importance. The inherent lack of dateable material in the hyperarid Atacama limits alternative chronological methods. Tephra layers represent a promising alternative, appearing across diverse sedimentary archives such as alluvial, fluvial, lacustrine, salar, and playa deposits (Sáez et al., 2012; Jordan et al., 2014; Vásquez et al., 2018; Medialdea et al., 2020; Ritter et al., 2022; Wennrich et al., 2025). Within the CRC1211, tephrochronology was used systematically to establish a time-stratigraphic framework for the Atacama Desert. These data are stored in a newly developed regionally focused tephra database, TephAta. TephAta can store a wide variety of tephra metadata, from field and lab context to physical, chemical and chronological characteristics. Storing the data in the dedicated TephAta database will facilitate the development of a regional tephrostratigraphic framework for the Atacama Desert. TephAta provides easy access to complex information that normally is distributed in several media (publications, private or public databases), hence fostering FAIR (findable, accessible, interoperable and reusable) data principals (Wilkinson et al., 2016). The design of TephAta is also meant to provide user friendly integration of suitable parts of the dataset (e.g. geochemical data) in global databases such as GEOROC (https://georoc.eu/) or the tephra-data-optimized EARTHCHEM (https://www.earthchem.org/) repository. This paper introduces the TephAta database and illustrates its usefulness by the presentation and discussion of an exemplary dataset obtained on widely distributed tephra deposits of Mid Pleistocene age from the central Atacama Desert.

2 The Central Volcanic Zone of the Andes

The subduction of the Farallon plate beneath the west coast of South America has caused continental arc volcanism within the Central Andes since Triassic times (Oliveros et al., 2018). The volcanic arc is characterized by low-flux, steady state andesitic magmatism and the construction of composite volcanoes (Burns et al., 2015). Starting about 25 Ma ago, an increase of the subduction rate and a shift in the subduction geometry of the Nazca Plate caused a eastward migration of the arc and associated crustal shortening and thickening (Allmendinger et al., 1997). This change is correlated with a shift to a high-flux, flare-up arc magmatism, which resulted in the production and eruption of large volumes of silicic "crustal" magmas (Wörner et al., 2018; Burns and De Silva, 2023). Ignimbrite volcanism is supposed to be not contemporaneous within the Central Volcanic Zone, indicating a north-south gradient towards younger major eruptive events (De Silva, 1989a; De Silva and Kay, 2018). The oldest ignimbrite deposits are incorporated within the Altos de Pica Formation (22-25 Ma; Jordan et al., 2014), the Oxaya Formation (19-23 Ma; Wörner et al., 2002; Van Zalinge et al., 2016) and the El Diablo Formations (11-16 Ma; Jordan et al., 2014). Between 10 and 1 Ma, magmatic fluxes strongly increased and numerous voluminous ignimbrites were erupted in pulses peaking at ca. 8.4 Ma, 5.5 Ma and 4.0 Ma (De Silva, 1989a; Sáez et al., 1999; Kay et al., 2010; Salisbury et al., 2011; Burns and De Silva, 2023). One of the most prominent surface morphologies of these ignimbrite deposits is the Altiplano-Puna Volcanic Complex (APVC) between 21 and 24°S (De Silva, 1989b). Subsequently, the high-flux volcanic activity waned and the construction of composite volcanoes and small-volume lava domes indicates the return to steady-state conditions (Burns and De Silva, 2023).

3 Database structure, samples, and analytical data

3.1 Database Structure

TephAta is hosted within the CRC1211 database (https://www.crc1211db.uni-koeln.de) and is focused entirely on storing and displaying information without data analysis by respective algorithms. In the backend, TephAta uses a relational database, MariaDB as data management system, communicating with a basic PHP instance hosted by the ITCC on virtual machines, while the frontend is handled by standard web technologies, with some display libraries (such as Tabulator or HighCharts) providing JavaScript interactivity. TephAta is designed to store field site and sample metadata of tephra samples in combination with respective analytical datasets. The data structure is adapted to the global tephra community guidelines for data acquisition and reporting outlined in Wallace et al. (2022). Data can originate from new investigations, but also from published work.

TephAta is organized into seven data categories: site, sample, physical properties, geochemistry, chronology, chronostratigraphy, and tephra correlations (Fig. 1a). A general introduction of the data stored in the different categories is given below and a full list and description of all input fields and upload functions is given in Supplementary Material.

The category "site" allows the documentation of sample location details including information about the site name, a general (log-) description, geographic position, physical habitus, and spatial context of an investigated location. The site category lists and links all samples taken from the same archive.

The section "sample" provides information when, how and by whom a sample from a specific site was taken. Further details about the sample type and material, its position within a site and the observed depositional processes can be defined. Information about sub- or split-samples and related (laboratory) labels can be listed together with the availability and accessibility of material and data. Specific analyses that were carried out can be indicated in an overview list.

The category "physical properties" collects field and microscopic observations. These include descriptions of the macrophysical properties of the stratigraphic layer (thickness, color, sedimentological structures, components), and its microphysical characteristics such as glass fragment morphology, mineral assemblages, or degree of alteration. Field sketches, images or notes and microscopic images can also be integrated.

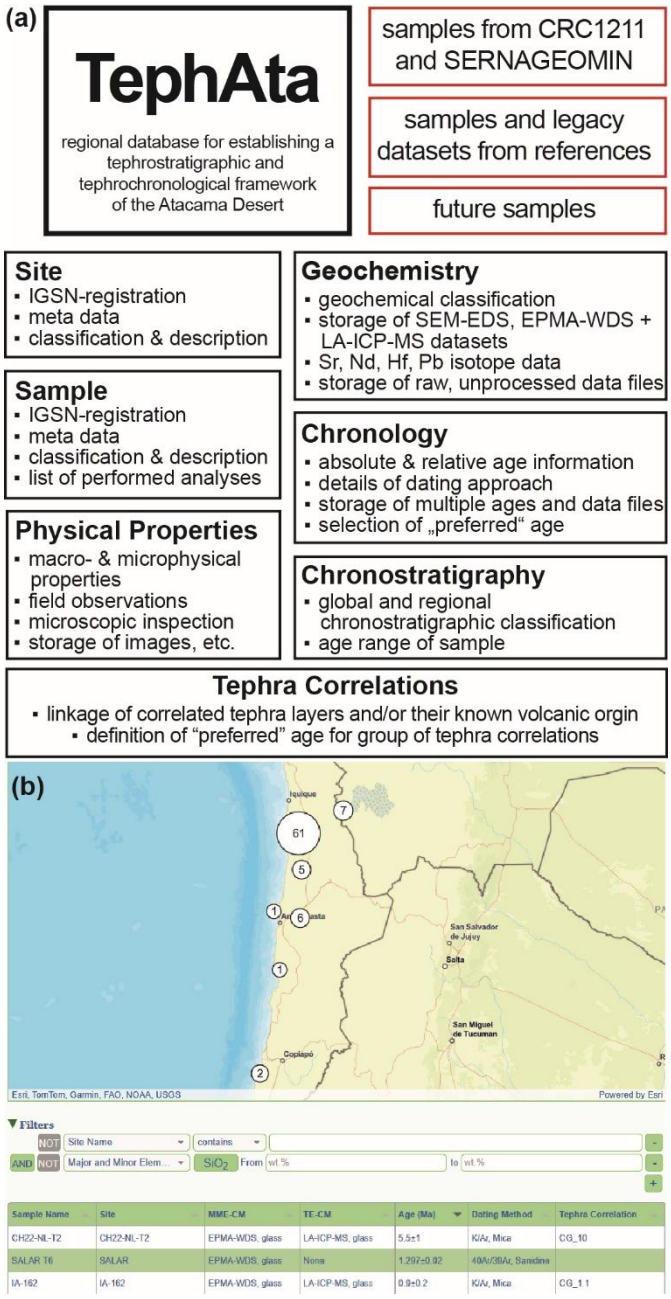

Figure 1: S (a) Structure of TephAta with its seven categories and different sources for data. (b) An example employing the sample filter function of TephAta showing the filtered samples on an interactive map and listing them below (CRC1211-TephAta, 2025). Map services and basemap provided by Esri via ArcGIS Online using data providers Esri, TomTom, Garmin, FAO, NOAA and USGS.

The “geochemistry” category facilitates the classification of volcanic rock types using the total alkali vs silica (TAS) classification (Le Bas et al., 1986). Geochemical datasets of major (>1 wt.%), minor (1-0.1 wt.%) and trace (<0.1 wt.%) element data, but also Sr, Nd, Pb isotope data can be archived. Unprocessed raw data, instrument log files and laboratory protocol data of geochemical analyses can be stored as supplementary files.

The “chronology” category collects age information related to a specific sample. Details on the applied dating technique(s) can be entered along with information about the dated material and specific age information (uncertainties, type of age calculation, xenocryst presence). Full analytical datasets including laboratory details as well as unprocessed and processed data-files (e.g., single crystal dating results) can be stored as supplementary files. For samples with multiple age determinations (e.g., by different dating techniques), users can designate a “best age”, to represent the most reliable age estimate in the sample overview.

Within the data category “chronostratigraphy” a specific sample can be categorized by its general (e.g. erathem, stage, etc.) and regional stratigraphic classifications. When available, this information is used to define minimum and maximum age

constraints. For samples which could be correlated with other tephra samples or a specific volcanic eruption by tephrostratigraphic means, a link between samples can be documented within "tephra correlations" category. Groups of correlated tephra can be further defined by a common name and their most reliable age. In case a tephra layer can be traced back to a specific volcanic origin, both the source volcano and eruption can be linked to the respective correlation.

All data is entered via the TephAta web interface (https://www.crc1211db.uni-koeln.de/tephata) using guided input forms, including unified predefined lists, as well as free-text fields for the input of individual data items. Geochemical data can be uploaded (and downloaded) using template data sheets provided on the website. The template files integrate sample and instrument metadata (e.g., sample IDs and types, related references, applied analytical protocols and instrument) with results from standards and samples, ensuring transparent documentation for interoperability and data reuse.

For all categories, additional data files (e.g., raw data and detailed instrument settings, field, and sample photo documentation) can be uploaded as zip-files. Datasets stored within TephAta can be continuously extended, as additional analyses become available. If no IGSN (International Generic Sample Number) was assigned to a site or sample before registration within TephAta, a new IGSN will be minted and connected with the internal metadata upon data submission in TephAta. The new IGSNs will be registered at the GFZ Data Services at the GFZ Helmholtz Centre for Geosciences and will then be associated with the TephAta URL, providing a link to the full metadata released within the database. Existing IGSN's can be linked to a sample during data submission. The IGSN enables a unique identification of a site and a sample and allows documentation outside TephAta including a connection to other databases. Data exchange to other global databases is also fostered by the structures of file templates, which are organized to match the needs of the global tephra-data repository EarthChem (https://www.earthchem.org/; Kuehn et al., 2023).

Datasets stored within TephAta can be accessed through the categories: "sites" and "samples". All data associated with a given sample or site are presented on a dedicated page that compiles and displays all shared entries. The sample list is linked to a map tool, which allows exploring entries within specific geographic areas (Fig. 1b). The sample list can be refined using combinable filters, including specific site sample and group of tephra correlations names (site name, sample name, lab ID, IGSN, name of group of tephra correlations). Users can also filter by the type of site (e.g., only alluvial fans), geochemical properties (TAS-classification, range of specific major, minor and/or trace element concentrations) and chronostratigraphic (series) and chronological (age range) values. Furthermore, users can select up to 15 samples to create compositional x-y plots. An overview of established tephra correlations is given by the "tephra correlations" list. These functions are designed to facilitate the identification of potential tephra correlations, providing the basis for detailed testing and subsequent establishment of tephrochronological frameworks.

Table 1: Overview table listing all sites and samples and respective IGSN included within TephAta along with information about their type of site, the availability of glass geochemical data (MME=major, minor elements, TE= trace elements), proposed age and dating details (if available, age and age uncertainty, dating method, dated mineral, dating laboratory, mineral standard and decay constant applied, type of age and reference of age). Further it is listed if the tephra was previously known and the sample was provided or (re-)sampled within the activities of the CRC1211, more details about the origin of samples are given within TephAta database. Sample AD-85 was provided by J. Quade (University of Arizona, USA) and sample TJ09-PdT-1 was provided by T. Jordan (Cornell University, USA).

References are:

1=Breitkreuz et al. (2014)
2= Placzek et al. (2009)
3 = Sáez et al. (2012)
4= Ritter et al. (2018)
5= this study
6= Gardeweg and Sellés (2013)
7= Astudillo et al. (2017)
8= Blanco and Tomlinson (2013)
9= Medina et al. (2012)
10=Escribano et al. (2013)
11= Marinovic et al. (1995)
12= Carrizo et al. (2008)
13=Vásquez et al. (2018)
14=Vásquez and Sepúlveda (2013)
15= Sepúlveda et al. (2014)
16= Rodríguez et al. (2015)
17= Horn (1991)
18=Wörner et al. (2000)
19= Medialdea et al. (2020)
20= Fornari et al. (2001)
21= Fritz et al. (2004)
22= Sepúlveda et al. (2023)
23= May et al. (2020)

site	sample	2nd sample name / resampled equivalent	IGSN	type of site	glass geochemical analyses	age (Ma)	age uncertainty (Ma)	dating method	dated mineral	dating laboratory	Ar-Ar mineral standard, decay constant	type of age	Refer-ence for age /sample	sample source	previously known or new sample
10-3-5-1	10-3-5-1	L-10	GF1211S-94	alluvial fan	MME + TE	not dated	not dated	N/A	N/A	N/A	N/A	N/A	1	reference	known
19MEJ9	19MEJ09	-	GF1211S-4E	alluvial fan	MME + TE	not dated	not dated	N/A	N/A	N/A	N/A	N/A	-	CRC	new
AD-1	AD-1	-	GF1211S-97	alluvial fan	MME + TE	0.750	0.060	$^{40}Ar/^{39}Ar$	biotite	Sernageomin	FC; Steiger & Jäger (1977)	plateau	2	reference	known
ARC	ARC1	-	GF1211S-44	alluvial fan	MME + TE	not dated	not dated	N/A	N/A	N/A	N/A	N/A	3	reference	known
Asche 4 / PAG-T4	PAG-T4	PAG Tephra 4	GF1211S--4	channel	MME + TE	0.980	0.040	U/Pb	zircon	University of Frankfurt	N/A	TuffZirc	4	CRC	new
Asche 4 / PAG-T4	PAG-T4	PAG Tephra 4	GF1211S--4	channel	MME + TE	0.301	0.007	$^{40}Ar/^{39}Ar$	biotite	University of Amsterdam	FC; Min et al. (2000)	weighted mean total fusion	5	CRC	new
ATA19-023 / CR-006	ATA19-023	CR-006A	GF1211S-3H	ignimbrite deposits	MME + TE	equivalent dated	equivalent dated	N/A	N/A	N/A	N/A	N/A	-	CRC	known
ATA19-023 / CR-006	CR-006A	ATA19-023	GF1211S-7C	ignimbrite deposits	-	0.280	0.014	$^{40}Ar/^{39}Ar$	biotite	Sernageomin	FC; Steiger & Jäger (1977)	plateau	6	reference	known
AVN-002	AVN-002d	-	GF1211S-33	alluvial fan	MME + TE	0.740	0.080	$^{40}Ar/^{39}Ar$	biotite	Sernageomin	FC; Steiger & Jäger (1977)	plateau	7	Sernageomin	known
C2-TEP-04 / IT93	C2-TEP-04	IT-93	GF1211S--Y	channel	MME + TE	equivalent dated	equivalent dated	N/A	N/A	N/A	N/A	N/A	-	CRC	known
C2-TEP-04 / IT93	IT-93	C2-TEP-04	GF1211S-7T	channel	-	0.170	0.040	$^{40}Ar/^{39}Ar$	biotite	Sernageomin	FC; Steiger & Jäger (1977)	plateau	8	reference	known
C2-TEP-05 / IT307	C2-TEP-05	IT-307	GF1211S-3-	channel	MME + TE	equivalent dated	equivalent dated	N/A	N/A	N/A	N/A	N/A	-	CRC	known
C2-TEP-05 / IT307	IT-307	C2-TEP-05	GF1211S-7U	channel	-	0.400	0.100	K-Ar	biotite	Sernageomin	Steiger & Jäger (1977)	N/A	8	reference	known
CC157 / L8 / 2/3/5/2	2/3/5/2	CC-157 // L8	GF1211S--7	alluvial fan	MME + TE	equivalent dated	equivalent dated	N/A	N/A	N/A	N/A	N/A	1	reference	known
CC157 / L8 / 2/3/5/2	CC-157	2/3/5/2 // L8	GF1211S-79	alluvial fan	-	0.230	0.130	$^{40}Ar/^{39}Ar$	biotite	Sernageomin	FC; Steiger & Jäger (1977)	inverse isochron	9	reference	known
CH17-001 (AD-85)	AD-85	CH17-001	GF1211S-7X	channel	MME	not dated	not dated	N/A	N/A	N/A	N/A	N/A	-	J. Quade	unknown
CH17-001 (AD-85)	CH17-001	AD-85	GF1211S-7-	channel	MME + TE	not dated	not dated	N/A	N/A	N/A	N/A	N/A	-	CRC	unknown
CH18-T1-4	CH18-T1	-	GF1211S-9M	alluvial fan	MME + TE	not dated	not dated	N/A	N/A	N/A	N/A	N/A	-	CRC	new
CH18-T1-4	CH18-T2	-	GF1211S-9N	alluvial fan	MME + TE	not dated	not dated	N/A	N/A	N/A	N/A	N/A	-	CRC	new

CH18-T1-4	CH18-T3	-	GF1211S-9P	alluvial fan	MME + TE	not dated	not dated	N/A	N/A	N/A	N/A	N/A	-	CRC	new
CH18-T1-4	CH18-T4	-	GF1211S-9R	alluvial fan	MME + TE	not dated	not dated	N/A	N/A	N/A	N/A	N/A	-	CRC	new
CH18-T5	CH18-T5	-	GF1211S-9T	alluvial fan	MME + TE	not dated	not dated	N/A	N/A	N/A	N/A	N/A	-	CRC	new
CH22-NL-T1	CH22-NL-T1	TPM-094	GF1211S--C	alluvial fan	-	3.900	0.800	$^{40}Ar/^{39}Ar$	biotite	Sernageomin	FC; Steiger & Jäger (1977)	combined isochron n=2	10	CRC	known
CH22-NL-T2	CH22-NL-T2	MAB-663	GF1211S--E	alluvial fan	MME + TE	5.500	1.000	K-Ar	biotite	Sernageomin	N/A	N/A	11	CRC	known
CH22-NL-T3	CH22-NL-T3-1	-	GF1211S--F	alluvial fan	-	not dated	not dated	N/A	N/A	N/A	N/A	N/A	-	CRC	known
CH22-NL-T3	CH22-NL-T3-2	-	GF1211S--H	alluvial fan	-	not dated	not dated	N/A	N/A	N/A	N/A	N/A	-	CRC	known
CHU / AN1	CHU Tephra	AN1	GF1211S-34	fault scarp	MME	equivalent dated	equivalent dated	N/A	N/A	N/A	N/A	N/A	-	Sernageomin	known
CHU / AN1	AN-1	CHU-Tephra	GF1211S-77	fault scarp	-	0.310	0.190	$^{40}Ar/^{39}Ar$	biotite	Sernageomin	N/A	plateau	12	reference	known
CHU-1	CHU-1	-	GF1211S-37	channel	MME	not dated	not dated	not dated	N/A	N/A	N/A	N/A	-	Sernageomin	known
CHU-2	CHU-2	-	GF1211S-39	badlands	MME	not dated	not dated	not dated	N/A	N/A	N/A	N/A	-	Sernageomin	known
CON-1	CON-1	-	GF1211S--9	channel	MME + TE	0.181	0.056	$^{40}Ar/^{39}Ar$	biotite	GEOMAR Kiel	TCR-2, unknown	plateau	3	reference	known
CTFON-4	CTFON-4	-	GF1211S-99	marine deposits	MME + TE	not dated	not dated	not dated	N/A	N/A	N/A	N/A	-	CRC	known
EL Rincon	19MEJ10	-	GF1211S-4F	marine deposits	-	not dated	not dated	N/A	N/A	N/A	N/A	N/A	-	CRC	new
EL Rincon	23MEJ1	-	GF1211S-4H	marine deposits	-	not dated	not dated	N/A	N/A	N/A	N/A	N/A	-	CRC	new
ESQ-1	ESQ-1	-	GF1211S--A	channel	MME + TE	0.151	0.033	$^{40}Ar/^{39}Ar$	biotite	GEOMAR Kiel	TCR-2	plateau	3	reference	known
GSQ-027	GSQ-027d	-	GF1211S-3X	terrace	MME + TE	0.255	0.017	$^{40}Ar/^{39}Ar$	biotite	Sernageomin	FC; Steiger & Jäger (1977)	plateau	13	Sernageomin	known
GSQ-08	GSQ-08d	-	GF1211S--J	terrace	MME + TE	0.300	0.020	$^{40}Ar/^{39}Ar$	biotite	Sernageomin	FC; Steiger & Jäger (1977)	plateau	13	Sernageomin	known
GSQ-106d	GSQ-106d	-	GF1211S-7E	alluvial fan	-	0.329	0.029	$^{40}Ar/^{39}Ar$	biotite	Sernageomin	FC; Steiger & Jäger (1977)	plateau	13	Sernageomin	known
GSQ-158	GSQ-158d	-	GF1211S--K	alluvial fan	MME + TE	0.340	0.021	$^{40}Ar/^{39}Ar$	biotite	Sernageomin	FC; Steiger & Jäger (1977)	plateau	13	Sernageomin	known
GSQ-53	GSQ-53d	-	GF1211S--L	alluvial fan	MME + TE	0.325	0.048	$^{40}Ar/^{39}Ar$	biotite	Sernageomin	FC; Steiger & Jäger (1977)	plateau	13	Sernageomin	known
GSV-132	GSV-132d	-	GF1211S-3M	fault scarp	MME + TE	0.140	0.057	$^{40}Ar/^{39}Ar$	biotite	Sernageomin	FC; Steiger & Jäger (1977)	plateau	13	Sernageomin	known
HU14/008 (IS-155)	HU14/008	IS-155	GF1211S-7Y	claypan	MME	equivalent dated	equivalent dated	N/A	N/A	N/A	N/A	N/A	-	CRC	known
HU14/008 (IS-155)	IS-155	HU14/008	GF1211S-7R	claypan	-	22.9	0.3	$^{40}Ar/^{39}Ar$	biotite	Sernageomin	FC; Steiger & Jäger (1977)	plateau	14	Sernageomin	known
HU17-014	HU17-014	-	GF1211S-9A	channel	MME + TE	not dated	not dated	N/A	N/A	N/A	N/A	N/A	-	CRC	new
HU18/001/002	HU18/001	-	GF1211S-4U	channel	MME + TE	not dated	not dated	N/A	N/A	N/A	N/A	N/A	-	CRC	new
HU18/001/002	HU18/002	-	GF1211S-4V	channel	MME	not dated	not dated	N/A	N/A	N/A	N/A	N/A	-	CRC	new
HU18-003 (IV-190)	HU18/003	IV-190	GF1211S-9-	channel	MME	equivalent dated	equivalent dated	N/A	N/A	N/A	N/A	N/A	-	CRC	known
HU18-003 (IV-190)	IV-190	HU18/003	GF1211S-7W	channel	MME + TE	0.620	0.040	$^{40}Ar/^{39}Ar$	biotite	Sernageomin	FC; Steiger & Jäger (1977)	plateau	14	Sernageomin	known
HU18-008 (IV-189)	HU18/008	IV-189	GF1211S-93	channel	MME	equivalent dated	equivalent dated	N/A	N/A	N/A	N/A	N/A	-	CRC	known
HU18-008 (IV-189)	IV-189	HU18-008	GF1211S-7V	channel	-	2.06	0.12	$^{40}Ar/^{39}Ar$	biotite	Sernageomin	FC; Steiger & Jäger (1977)	inverse isochron	14	reference	known
IA-05	IA-05	-	GF1211S-7F	alluvial fan	-	0.40	0.20	K-Ar	biotite	Sernageomin	FC; Steiger & Jäger (1977)	combined K-Ar n=2	15	Sernageomin	known
IA-105	IA-105	-	GF1211S-7H	alluvial fan	-	0.314	0.012	$^{40}Ar/^{39}Ar$	biotite	Sernageomin	FC; Steiger & Jäger (1977)	plateau	15	Sernageomin	known
IA-11	IA-11	-	GF1211S--M	channel	MME + TE	0.430	0.040	$^{40}Ar/^{39}Ar$	biotite	Sernageomin	FC; Steiger & Jäger (1977)	inverse isochron	15	Sernageomin	known
IA-120	IA-120	-	GF1211S--N	alluvial fan	MME + TE	0.300	0.200	K-Ar	biotite	Sernageomin	FC; Steiger & Jäger (1977)	combined K-Ar n=2	15	Sernageomin	known
IA-137	IA-137	-	GF1211S-7J	channel	-	0.700	0.400	K-Ar	biotite	Sernageomin	FC; Steiger & Jäger (1977)	N/A	15	Sernageomin	known

IA-162	IA-162	-	GF1211S--P	alluvial fan	MME + TE	0.900	0.200	K-Ar	biotite	Sernageomin	FC; Steiger & Jäger (1977)	combined K-Ar n=2	15	Sernageomin	known
CH22-NL-T46	CH22-NL-T46	IA-270?	GF1211S-3W	hillslope	MME	equivalent dated	equivalent dated	N/A	N/A	N/A	N/A	N/A	-	CRC	known
IA-270	IA-270	CH22-NL-T46?	GF1211S-7K	alluvial fan	-	0.410	0.030	$^{40}Ar/^{39}Ar$	biotite	Sernageomin	FC; Steiger & Jäger (1977)	plateau	15	Sernageomin	known
IA-95	IA-95	-	GF1211S-7L	alluvial fan	-	0.500	0.300	K-Ar	biotite	Sernageomin	FC; Steiger & Jäger (1977)	N/A	15	Sernageomin	known
IA-97	IA-97	-	GF1211S-7M	alluvial fan	-	0.600	0.300	K-Ar	biotite	Sernageomin	FC; Steiger & Jäger (1977)	combined K-Ar n=2	15	Sernageomin	known
IQ18-001	IQ18-001	-	GF1211S-9E	alluvial fan	MME + TE	not dated	not dated	N/A	N/A	N/A	N/A	N/A	-	CRC	known
IQ18-002(CMI13.3)	CMI13.3	IQ18-002	GF1211S-7A	alluvial fan	-	0.700	0.110	$^{40}Ar/^{39}Ar$	biotite	Sernageomin	FC; Steiger & Jäger (1977)	plateau	14	Sernageomin	known
IQ18-002 (CMI13.3)	IQ18-002	CMI13.3	GF1211S-9C	alluvial fan	MME + TE	equivalent dated	equivalent dated	N/A	N/A	N/A	N/A	N/A	-	CRC	known
IR22-01	IR22-001	-	GF1211S--T	ignimbrite deposits	MME + TE	not dated	not dated	N/A	N/A	N/A	N/A	N/A	-	CRC	known
IR22-02	IR22-002	-	GF1211S-3A	ignimbrite deposits	MME + TE	not dated	not dated	N/A	N/A	N/A	N/A	N/A	-	CRC	known
IRRU-13	IRRU-13	-	GF1211S-4A	flank of volcano	MME	not dated	not dated	N/A	N/A	N/A	N/A	N/A	16	reference	known
IRRU-46a	IRRU-46a	-	GF1211S-7N	flank of volcano	-	0.258	0.049	$^{40}Ar/^{39}Ar$	biotite	Oregon State University	FC	inverse isochron	16	reference	known
IRU-15	IRU-15	-	GF1211S-7P	ignimbrite deposits	-	0.320	0.250	K-Ar	biotite	NERC	N/A	plateau	17, 8	reference	known
IRU-1a	IRU-1a	-	GF1211S-4C	flank of volcano	MME + TE	0.181	0.009	$^{40}Ar/^{39}Ar$	biotite	University of Amsterdam	FC; Min et al. (2000)	weighted mean total fusion	5, 17, 18	reference	known
PAG	PAG17 ID14	-	GF1211S-4R	claypan	MME	not dated	not dated	N/A	N/A	N/A	N/A	N/A	-	CRC	new
PAG	PAG17 ID24	-	GF1211S-4T	claypan	MME	not dated	not dated	N/A	N/A	N/A	N/A	N/A	-	CRC	new
PAG	PAG17 ID4	-	GF1211S-4P	claypan	MME	not dated	not dated	N/A	N/A	N/A	N/A	N/A	-	CRC	new
PAG	PAG17 ID54	-	GF1211S--3	claypan	MME	not dated	not dated	N/A	N/A	N/A	N/A	N/A	-	CRC	new
PAG T-1-2	PAG-T1	PAG Tephra1	GF1211S-9K	claypan	MME + TE	not dated	not dated	N/A	N/A	N/A	N/A	N/A	-	CRC	new
PAG T-1-2	PAG-T2	PAG Tephra 2	GF1211S-9L	channel	MME + TE	not dated	not dated	N/A	N/A	N/A	N/A	N/A	-	CRC	new
PAG17.2008	PAG17.2-008	-	GF1211S-4J	channel	MME + TE	not dated	not dated	N/A	N/A	N/A	N/A	N/A	-	CRC	new
PAG17/001	PAG17/001	-	GF1211S--U	alluvial fan	MME + TE	not dated	not dated	N/A	N/A	N/A	N/A	N/A	-	CRC	new
PAG17/006	PAG17/006	-	GF1211S-9F	channel	MME + TE	not dated	not dated	N/A	N/A	N/A	N/A	N/A	-	CRC	new
PAG17/027	PAG17/027	-	GF1211S-9H	channel	MME + TE	not dated	not dated	N/A	N/A	N/A	N/A	N/A	-	CRC	new
PAG18/001	PAG18/001	-	GF1211S--V	channel	MME + TE	not dated	not dated	N/A	N/A	N/A	N/A	N/A	-	CRC	new
PAG18/002	PAG18/002	-	GF1211S-47	alluvial fan	MME + TE	not dated	not dated	N/A	N/A	N/A	N/A	N/A	-	CRC	new
PAG18/003	PAG18/003	-	GF1211S-49	alluvial fan	MME + TE	not dated	not dated	N/A	N/A	N/A	N/A	N/A	-	CRC	new
PAG18/008	PAG18/008	-	GF1211S-9J	channel	MME + TE	not dated	not dated	N/A	N/A	N/A	N/A	N/A	-	CRC	new
POR 3	POR 3	-	GF1211S-3J	flank of volcano	MME + TE	0.290	0.450/0.290	K-Ar	feldspar	NERC	Steiger and Jager, 1977	No reliable ages	17, 18	reference	known
POR 3	POR 3	-	GF1211S-3J	flank of volcano	MME + TE	0.150	0.200/0.150	K-Ar	biotite	NERC	Steiger and Jager, 1977	No reliable ages	17, 18	reference	known
QP	QP1	-	GF1211S-4-	channel	MME + TE	not dated	not dated	N/A	N/A	N/A	N/A	N/A	3	reference	known
QP	QP4	-	GF1211S-43	channel	MME + TE	not dated	not dated	N/A	N/A	N/A	N/A	N/A	3	reference	known
Quebrada Ancha	Tephra RB	-	GF1211S--X	channel	MME + TE	not dated	not dated	N/A	N/A	N/A	N/A	N/A	-	CRC	new
Quebrada Tiburón - Section A	TIB4-TEPH1	-	GF1211S-4W	marine deposits	MME + TE	not dated	not dated	N/A	N/A	N/A	N/A	N/A		CRC	new
Quebrada Tiburón - Section A	TIB4-F2	-	GF1211S-4X	marine deposits	MME + TE	not dated	not dated	N/A	N/A	N/A	N/A	N/A		CRC	new
RL North	Tephra RL N	-	GF1211S-3Y	alluvial fan	MME + TE	not dated	not dated	N/A	N/A		N/A	N/A	-	CRC	new
SALAR	SG17/001	SALAR T6	GF1211S-4K	hillslope	MME	equivalent dated	equivalent dated	N/A	N/A	N/A	N/A	N/A	-	CRC	new
SALAR	SG17/002	SALAR T4	GF1211S-4L	hillslope	MME	equivalent dated	equivalent dated	N/A	N/A	N/A	N/A	N/A	-	CRC	new

SALAR	SG17/003	SALAR T2	GF1211S-4M	hillslope	MME	equivalent dated	equivalent dated	N/A	N/A	N/A	N/A	N/A	-	CRC	new
SALAR	SALAR T6	SG17/001	GF1211S-3V	hillslope	MME	1.297	0.018	$^{40}Ar/^{39}Ar$	sanidine	University of Amsterdam	FC; Min et al., 2000	weighted mean total fusion	19	CRC	new
SALAR	SALAR T6	-	GF1211S-3V	hillslope	MME	0.098	0.015	indirect - sediment OSL dating + absolute	N/A	University of Cologne	N/A	AGE-MODEL	19	CRC	new
SALAR	SALAR T5	-	GF1211S-3U	hillslope	MME	0.084	0.008	indirect - sediment OSL dating	N/A	University of Cologne	N/A	AGE-MODEL	19	CRC	new
SALAR	SALAR T4	SG17/002	GF1211S-3T	hillslope	MME	0.083	0.009	indirect - sediment OSL dating	N/A	University of Cologne	N/A	AGE-MODEL	19	CRC	new
SALAR	SALAR T3	-	GF1211S-3R	hillslope	-	0.072	0.008	indirect - sediment OSL dating	N/A	University of Cologne	N/A	AGE-MODEL	19	CRC	new
SALAR	SALAR T2	SG17/003	GF1211S-3P	hillslope	MME + TE	0.071	0.007	indirect - sediment OSL dating	N/A	University of Cologne	N/A	AGE-MODEL	19	CRC	new
SALAR	SALAR T1	-	GF1211S-3N	hillslope	MME + TE	0.068	0.008	indirect - sediment OSL dating	N/A	University of Cologne	N/A	AGE-MODEL	19	CRC	new
Salar de Uyuni - C1986	L5	TSdU	GF1211S-3K	salar	-	0.191	0.005	$^{40}Ar/^{39}Ar$	biotite	Université de Nice — Sophia-Antipolis	Bern 4B biotite, N/A	fusion + isochron	20	reference	known
Salar de Uyuni - C1999	TSdU	L5	GF1211S-3L	salar	MME + TE	0.059	n/a	indirect U/Th of host sediment	halite	University of California?	N/A	AGE-MODEL	21	reference	known
SMS-15d	SMS-15d	-	GF1211S--W	channel	MME + TE	0.375	0.017	$^{40}Ar/^{39}Ar$	biotite	Sernageomin	FC; Steiger & Jäger (1977)	plateau	22	Sernageomin	known
T3	SGL3	-	GF1211S-3F	alluvial fan	MME	0.080	n/a	indirect - sediment OSL dating	N/A	University of Cologne	N/A	AGE-MODEL	23	CRC	new
TA-7-8	TA-8	-	GF1211S-3E	channel	MME	0.210	0.066	$^{40}Ar/^{39}Ar$	biotite	GEOMAR Kiel	TCR-2	plateau	3	reference	known
TA-7-8	TA-7	-	GF1211S-3C	channel	MME	0.098	0.042	$^{40}Ar/^{39}Ar$	biotite	GEOMAR Kiel	TCR-2	plateau	3	reference	known
TJ09-PdT1	TJ09-PdT1	-	GF1211S-4N	playa	MME + TE	not dated	not dated	N/A	N/A	N/A	N/A	N/A	-	T. Jordan	unknown
TOC14/001	TOC14/001	-	GF1211S--R	alluvial fan	MME + TE	not dated	not dated	N/A	N/A	N/A	N/A	N/A	-	CRC	new

220

3.2 Samples and chronological and geochemical data

TephAta focuses on tephra samples from the Atacama Desert and adjacent regions, namely the Coastal Cordillera, the Central Depression, Precordillera and parts of the Western Cordillera regardless of their age. To date, the dataset primarily includes 225 samples from the late Middle Pleistocene to Late Pleistocene, largely collected during field campaigns within the CRC1211 (2013-2023). These samples are derived from sites, which were within the scientific focus areas of CRC1211 subprojects and adjacent sites to create a broad data foundation for characterizing major eruptive events and developing a tephrochronological framework. This set of samples was augmented by identifying tephra sites on geological maps and/or described in literature. Where tephra layers were identified near investigated CRC1211 archives or shared similar ages, sample splits were requested 230 from the Chilean National Geology and Mining Survey (SERNAGEOMIN) or the respective researchers of literature sources. If material could not be provided, respective sample sites were revisited and resampled during field CRC1211 field campaigns. TephAta also allows the integration of legacy data for samples that are not accessible. Given their diverse origins across different projects and decades, the currently investigated samples lack a standardized initial collection protocol. Consequently, TephAta has been designed to accommodate this heterogeneity within a unified framework by offering a comprehensive set

of optional data fields that can be utilized as information becomes available. Metadata and morphological field descriptions were extracted from references, field notes, or provided by personal communication.

Chronological data

Available ages for the samples currently included in TephAta have been extracted from published data and were complemented by new chronological results. Available ages from literature were obtained by $^{40}Ar/^{39}Ar$, K-Ar and U-Pb dating, but also inferring indirect tephra ages by dating the host sediment. Available details of the respective dating techniques, age calculations and references are stored sample-specific within TephAta and are summarized in Table 1.

For two samples (PAG-T4 and IRU-1a) new ages were obtained by $^{40}Ar/^{39}Ar$ multi-grain fusion dating of biotite at the Vrije Universiteit Amsterdam and are presented here for the first time. Mineral separates were achieved by sieving, magnetic separation, and hand picking before the selected mineral separate was packed in a 6 mm ID AI packages and loaded in a 25 mm ID Al cup together with Fish Canyon Tuff sanidine (FCs) standard. Sample and standard were irradiated at the Oregon State University TRIGA reactor in the cadmium shielded CLICIT facility for 7 hours (irradiation code VU114 and 15-OSU-06). At Vrije Universiteit Amsterdam after irradiation, samples and standards were unpacked and loaded in a 185 hole Cu tray and baked overnight at 250 °C under vacuum. This tray was then placed in a doubly pumped vacuum chamber with Zn-Se window and baked overnight at 120 °C under high vacuum. This chamber is connected to a ThermoFisher NGPrep gas purification line equipped with a hot GP50, a cold finger (Lauda at -70 °C) and hot St707 getter. Samples (1-3 grains/fusion) and standards (1 grain/fusion) are fused using a 25 W Synrad CO_2 laser. Released gas is analyzed on an ARGUS VI+ noble gas mass spectrometer, equipped with four Faraday cups at the H2, H1, AX and L1 positions and two compact discrete dynodes (CDDs) at positions L2 and L3. The system is equipped with a 1012 Ohm amplifier on H2 and 1013 Ohm amplifiers on H1, AX and L1 cups. Samples were run on H1-L3 collectors. Similar to Phillips and Matchan (2013), no bias corrections were applied, but samples and standards were analyzed in the same tray (and thus at more or less the same time) alternating with air pipettes with intensities in the same range as the samples and standards. Line blanks were measured every 2-3 unknowns and were subtracted from succeeding sample data. Data reduction is done in ArArCalc (Koppers, 2002). Ages are calculated with decay constants of Min et al. (2000) and 28.201 Ma for FCs (Kuiper et al., 2008). The atmospheric $^{40}Ar/^{36}Ar$ air value of 298.56 is used (Lee et al., 2006). The correction factors for neutron interference reactions are $(2.64 \pm 0.02) \times 10^{-4}$ for $(^{36}Ar/^{37}Ar)$ Ca, $(6.73 \pm 0.04) \times 10^{-4}$ for $(^{39}Ar/^{37}Ar)$ Ca, $(1.21 \pm 0.003) \times 10^{-2}$ for $(^{38}Ar/^{39}Ar)$ K and $(8.6 \pm 0.7) \times 10^{-4}$ for $(^{40}Ar/^{39}Ar)$ K. All errors are quoted at the 2σ level.

Geochemical data

Depending on individual sample properties, different preparation methods were applied to enrich volcanic glass fragments for geochemical analyses. These methods include classical preparation techniques, like crushing of lithified/solidified samples, rinsing, (wet-) sieving, magnetic and density separation, and hand picking. Specific information for each sample is listed in the sample description and is also given along with the analytical results within the data-files provided for download (e.g., results of geochemical analyses). Respective aliquot fractions enriched in glass fragments were mounted on epoxy pucks and polished to remove potential surficial alteration and to avoid topographic effects causing compositional variations during subsequent glass geochemical analyses.

The pucks were carbon coated for major and minor element analyses of glass by electron probe microanalysis (EPMA) wavelength dispersive spectroscopy (WDS) and/or scanning electron microscope energy dispersive spectroscopy (SEM-EDS). Specific methodological details for each sample are provided alongside the geochemical datasets in TephAta.

A JEOL JXA-8900RL electron microprobe equipped with five-wavelength dispersive spectrometers was used for these analyses at the University of Cologne (UoC). The operation conditions were set to 12 kV accelerating voltage, 6 nA beam

current and 5 µm beam diameter. Full details of calibration and measuring conditions are given in Leicher (2021). Data reduction included ZAF correction and substitution of halogens (Cl, F) for oxygen using the JEOL Ltd JXA8900 Basic Software V3.02. Only EPMA-WDS geochemical analyses of glass fragments with analytical totals >90 wt.% were considered and normalized to 100% on a loss on ignition free basis, excluding volatiles (Cl, SO_3 and F).

A Zeiss Sigma 300-VP equipped with an OXFORD Instruments EDX detector controlled by the software Aztec 4.1 was used for SEM-EDS analyses, at the UoC. The instrument was set to 20 keV and an image resolution of 512*512 pixel was chosen. The number of channels was set to 2048, processing time to 5, with a dwell time of 10000 µs. The size of the scanning frame was adjusted to the respective grain size and typically exceeded 10 µm.

Trace-element analyses of glass fragments were performed at the University of Bonn (UoB) and UoC on the same sample pucks as the EPMA-WDS/SEM-EDS analyses, after removing the carbon coating. At the UoB trace element analyses were performed using a Resonetics Resolution M50E 193 nm excimer laser ablation system coupled to a Thermo Scientific Element XR (Leicher and Lagos, 2021). A spot size of 26 µm was chosen and analyses were performed at a repetition rate of 5 Hz and a count time of 35 sec on the sample after 30 sec on the gas blank (background). A He gas flow (0.75 l min^{-1}), mixed together with Ar sample gas (~1.1 l min^{-1}) transported ablated material via an in-house signal-smoothing device to the ICP-MS. Maximum intensity as well as stability of the signal were obtained by tuning while taking account of concurrently low oxide ratios (ThO/Th of ~0.0012) to minimize potentially interfering oxide species prior to analyses in low-resolution mode. At UoC an NWRimageGEO 193 nm ArF excimer laser ablation system coupled to a Thermo Scientific iCAP quadrupole or iCAP triple quadrupole ICP-MS was used for trace-element analyses. Individual glass fragments were analyzed using 15 or 20 µm spot size, a repetition rate of 6 Hz and a count time of 40 sec on the sample after 30 sec of the gas blank (background) measurements. The sample aerosol was taken up by a He gas flow (0.9 l min^{-1}) and mixed with Ar (0.8 l min^{-1}), within a glass smoothing device before introduction into the plasma.

All data reduction was performed using the software Iolite 4.3 (Paton et al., 2011). The standard glass NIST SRM 612 was used for calibration and calculation of trace element concentrations based on ^{43}Ca, ^{85}Rb, ^{88}Sr, ^{89}Y, ^{90}Zr, ^{93}Nb, ^{138}Ba, ^{139}La, ^{140}Ce, ^{141}Pr, ^{146}Nd, ^{147}Sm, ^{153}Eu, ^{157}Gd, ^{159}Tb, ^{163}Dy, ^{165}Ho, ^{166}Er, ^{169}Tm, ^{172}Yb, ^{175}Lu, ^{178}Hf, ^{181}Ta, ^{208}Pb, ^{232}Th, ^{238}U. As an internal standard ^{29}Si was incorporated using median SiO_2 concentrations obtained from EPMA-WDS data of respective samples. Since major and minor elements such as Ti, Na, K, or P were not analyzed by LA-ICP-MS, they could not be considered for detection of potential contamination by mineral phases during ablation. However, during data reduction in Iolite, the full analyzed trace element spectrum and Ca were screened to identify and exclude potential mineral inclusions (e.g. relatively elevated Ca, Sr, or Ba counts indicating feldspar inclusions) from data selection.

The here presented geochemical data can be either downloaded as sample-specific datasets from the TephAta database (https://www.crc1211db.uni-koeln.de/tephata) or can be found as a combined dataset of all samples deposited at EarthChem (Leicher N., 2026).

Data quality of geochemical analyses

During EPMA-WDS, SEM-EDS and LA-ICP-MS analysis MPI-DING standard glasses (ATHO-G, StHs6/80-G; Jochum et al., 2006) and SRM NIST SRM 610 (Jochum et al., 2011) were used as secondary standards to evaluate the accuracy and precision of individual measurement sessions. Sample-specific results of secondary standard analysis are stored within TephAta along with the sample results and are provided for download within the sample-specific data-file.

Over the full analytical period, EPMA-WDS analyses conducted at UoC yielded mean intermediate precision (expressed as relative two standard deviation) and accuracy (expressed as bias relative to the preferred reference value) of up to 2.5 and 0.6 %, respectively, for elemental concentrations >75 wt.%, up to 4.4% and 0.6% for 75-12 wt.%, up to 13.33 % and 2.0 % for 12-1 wt.% and up to 58.4 % and 6.4 % for <1 wt.%. Mean values for intermediate precision and accuracy of SEM-EDS

analyses, are up to 0.6 and 0.3% for elemental concentrations > 75 wt.%, up to 3.8 % and 0.3 % for 75-12 wt.%, up to 18.0 % and 3.7 % for 12-1 wt.% and up to 60.0 % and 7. 9 % for <1 wt. %.

Secondary standard analyses of MPI-DING glasses ATHO-G and StHs6/80-G during LA-ICP-MS analyses at the UoB revealed median intermediate accuracies of <5 % for Sm, Ho, Rb, Ba, Pr, Ca, Sr, Ce, Yb, Lu, Hf, and Er, 5-12 % for La, Dy, Nd, Tm, U, Tb, Th, Eu, Y, Zr, Gd, Nb and Ta and 19 % for Pb. The median intermediate precision of the secondary standard analyses at UoB was typically <10 % for Sr, Zr, Ce, Nb, Rb, Ba, La, Ca, Pr, Y, and Th and 10-28 % for Nd, U, Hf, Er, Ho, Pb, Dy, Eu, Gd, Ta, Sm, Tb, Lu, Yb, and Tm. At the UoC, secondary standard analyses of MPI-DING glasses (ATHO-G, StHs6/80-G) glasses during LA-ICP-MS analyses revealed median accuracies of 5-10 % for Rb, Sr, Ba, Ca, Ce, La, Sm, Ho, and U, 10-15 % for Zr, Nd, Th, Hf, Y, Pr, Eu, Tb, Er, Yb, Nb, Dy Pb and 15-17 % for Gd, Lu, Tm and Ta. The median intermediate precision of the secondary standard analyses at UoC was typically < 10 % for Sr, Ba, Zr, Ce, La, Rb, Nb, Y, Ca, Pr, Nd, Th, Hf, Yb, U, Pb, Er, and Ta and of 10-16 % for Ho, Gd, Sm, Dy, Tb, Eu, Lu, and Tm.

4 Results and Discussion

4.1 Site and sample data

Currently, the TephAta dataset lists 106 tephra samples from 91 tephra deposits sampled at 74 sites between approximately 20 – 27° S to 70-67°W. The specific origin (locality, reference) of samples is listed in Table 1. The set of samples includes 65 samples taken before the CRC-research activities of which 23 samples originate from mapping campaigns of the SERNAGEOMIN and 25 samples from other regional geoscientific studies. In addition, 17 previously known sample sites were revisited and re-sampled as part of the CRC's field work during which 41 newly identified tephra samples were gathered and included here.

Tephra samples are sourced from all types of sediment deposits of the Atacama Desert including alluvial fans, river terraces as well as clay pan and halite deposits. In addition, a small set of samples originating from the proximal deposits associated with the Irruputuncu volcanic complex were included, because they represent a potential volcanic source. Sampling sites are mostly outcrops formed by the incision of channels, gravimetric movement, tectonic activity, and roadcuts, and also include pits and drill cores. Tephra deposits show a broad variety in their physical properties, which represents the variable influence of eruption parameters and (post-) depositional related processes. The typical thickness of tephra layers is in the scale of centimeters, but also include several m-thick to sub-cm thin tephra deposits, whose lateral extent ranges from decimeter to hectometer. In addition, cryptotephra horizons have been identified in sediment cores. Visible volcanic ash layers are most commonly of bright color. Sedimentological texture properties, such as the grain-size, are in the range of ash (<2 mm diameter) for most tephra deposits, due to their distance to potential source volcanoes. Internal sedimentological structure of these tephra deposits, like grading, are only rarely observed due to their generally well-sorted grain-size distribution and are, if observed, commonly related to post-depositional weak water current transport processes. The mineralogical composition of tephra layers is dominated by glass, but also primary (biotite, feldspar, zircon) and secondary minerals (gypsum, halite) were observed. The level of details of the available morphological description of individual layers varies, as for some samples morphological and mineral compositional details are incomplete.

4.2 Chronology of samples

Biotites of sample PAG-T4 were $^{40}Ar/^{39}Ar$ dated in two analytical sessions (19T04: n=10; 1-3 grains/hole; 19T11: n=20; 10 grains/hole) yielding individual weighted mean ages of 318.8 ± 18.9 ka (n=7 ages) and 298.4 ± 7.4 ka (n=18 ages), with a combined weighted mean age of 301.3 ± 13.8 ka. The weighted mean age is obtained by including as many individual analyses with mean squared weighted deviation (MSWD) < T-test statistic at 95 % confidence level. The $^{40}Ar/^{36}Ar$ inverse isochron intercept is 297.9 ± 1.0 and overlaps with air values of Lee et al. (2006). The analytical errors in the first series are larger due to small beam intensities. The radiogenic ^{40}Ar yield is on average ~4 %. Biotites of sample IRU-1a were analyzed during the

same analytical sessions (19T04: n=10; 1-3 grains/hole; 19T11: n=20; 4-5 grains/hole) as samples of PAG-T4 and their weighted mean age computation followed the same criteria. The first series yielded a weighted mean age of 188.7 ± 12.1 ka (n=6 ages) and the second series 171.2 ± 12.6 ka (n=7 ages), which gives a combined weighted mean of 180.5 ± 8.7 ka. The $^{40}Ar/^{36}Ar$ inverse isochron intercept is 298.1 ± 0.6 and overlaps with air values of Lee et al. (2006). The radiogenic ^{40}Ar yield is very low with ~2 % on average. In the second series, parts of the experiments were discarded because the ^{40}Ar signal was too high for the detector and runs were aborted.

In combination with the data available in literature, 42 direct tephra ages obtained by absolute dating methods and 8 indirect tephra ages obtained by luminescence or U-Th dating of the host sediment, are available for 47 of 106 samples (Table 1, 3 samples have multiple ages). Of the 42 direct ages, the majority derives from biotite $^{40}Ar/^{39}Ar$ dating (n=29), whereas the other ages were obtained by biotite K-Ar (n=10), feldspar K-Ar (n=1), feldspar $^{40}Ar/^{39}Ar$ (n=1) and zircon U-Pb (n=1) dating methods.

The samples so far included in TephAta cover an age range from 22.90 to 0.06 Ma. Most samples (n=45) have an age < 1 Ma, but few samples (n=5) have Early Pleistocene to Miocene ages (Ritter et al., 2018; Medialdea et al., 2020). The ages of tephra layers >1 Ma suggest several distinct eruptive events, whereof only the ages of two samples partly overlap due to their uncertainties of up to 21 % (CH22-NL-T1 and -T2, cf. Table 1). The $^{40}Ar/^{39}Ar$ sanidine of tephra layer SALAR T6 age (1.297±0.018 Ma) is contradicted by a much younger IRSL host sediment age (<0.1 Ma), which is discussed in detail below.

Among the <1 Ma old tephra layers, two main periods of explosive volcanic activity can be tentatively identified within the dataset (Fig. 2a). The older period includes tephra with ages of 0.9-0.5 Ma (n=7) and clustering between 0.75 and 0.60 Ma. The younger period includes samples with continuously overlapping ages between 0.43 and 0.06 Ma (n=36). One tephra deposit (PAG-T4) could not be assigned to one of these two periods, as different dating techniques provide very different ages with the new $^{40}Ar/^{39}Ar$ biotite age of 0.301±0.007 Ma and an U-Pb zircon age of 0.98 ± 0.04 Ma (Ritter et al., 2018). In general the active periods were also identified based on a partly overlapping dataset of chronological data focusing on tephra layers of the Coastal Cordillera of 20-21° S (Sepúlveda et al., 2013; Quezada et al., 2018).

Using solely the chronological data within the TephAta dataset to disentangle and identify individual volcanic events <1 Ma within the two periods of volcanic activity is challenging. The heterogeneous dating techniques applied within several decades (1978-2023) used a variety of instruments, protocols, internal standards, and respective reference values, which limit the accurate differentiation of similar ages. A homogenization, e.g., through recalculation of ages based on the same reference values for mineral standards and decay constants, to increase the comparability of the complete dataset is, however, hampered by scarcity of metadata and is further limited by the fact that different dating methods have been applied. Besides the uncertainties related to the different methodological approaches, also the sample-specific aspects (quantity and quality of minerals, type of target minerals, plateau vs isochrone ages) infer further ambiguity in comparing their ages. 20 samples have relatively large age uncertainties of more than >15 %, which is especially evident within the group of K-Ar ages. Furthermore, due to uncertainties exceeding the respective dated ages, some (n=2) ages have to be classified as unreliable.

The ages of 7 samples assigned to the older period (0.5-0.9 Ma) overlap among each other within their uncertainties and do not allow a further differentiation. Among the younger sample group (<0.5 Ma), relatively small uncertainties of a few ages (SMS-15d: 0.375±0.017 Ma, GSQ-08d: 0.300±0.020 Ma, GSQ-027d: 0.255±0.017 Ma, TdSU: 0.191±0.005 Ma and IRU-1a: 0.181±0.009 Ma) indicate a potential chronological differentiation into multiple eruptive events. All other ages of tephra layers, however, widely overlap with the aforementioned more precise ages and among each other, which hampers the assignment of tephra to a specific eruptive event. The age differences between some samples are within a range of 1-2 ka (e.g., GSQ-158d: 0.361-0.319 Ma vs GSQ-08d: 0.320-0.280 Ma; Fig. 2a), which is too small for a clear differentiation between eruptive events. Moreover, also the accuracy of the (more precise) ages is difficult to assess as their ages are based on a single, multi-grain incremental heating experiment, from which a plateau age was calculated. This limits the detection of sources for potential biases such as xenocryst contamination, incorporation of altered minerals or minerals with a complex crystallization history

(Hora et al., 2010; Kern et al., 2016). Such biases are suggested for some samples, whose $^{40}Ar/^{36}Ar$ values are above the uncertainties of the atmospheric air value and thus indicate excess Ar, so that only inverse isochrone ages could be computed (e.g., IA-11, SMS-15d). Considering the few available total fusion ages within the dataset (PAG-T4, IRU-1a), their individual ages show a natural scatter in ages and thus provide additional information to extrapolate more robust eruption ages, while potential biased ages (e.g. several age populations caused by xenocrysts) can be filtered. Among the here listed samples, only very few samples have been dated by different dating approaches to further test for potential biases. The available results indicate inconsistencies such as by the zircon U-Pb age for tephra PAG-T4 of 0.98±0.04 Ma (Ritter et al., 2018), which is in conflict with the $^{40}Ar/^{39}Ar$ biotite age of 0.301±0.06 Ma obtained from the same sample. The youngest tephra ages included in the dataset derive from a series of indirect infrared stimulated luminescence (IRSL) ages of the respective outcrop. The stratigraphic oldest tephra layer of this deposit (SALAR T6) has been also dated by sanidine $^{40}Ar/^{39}Ar$ (Medialdea et al., 2020) yielding a weighted mean age of 1.297±0. 018 Ma is based on a robust population of 25 individual total fusion ages. However, this age is much older than the proposed IRSL maximum age <0.098±0.015 Ma and was explained by the authors as a potential reworking of the tephra layer (Medialdea et al., 2020). New tephrostratigraphic conclusions based on new geochemical signatures (discussed below), however, question this hypothesis. Further, the geochemical fingerprint of an overlying tephra (SALAR-T2) in the succession likely corresponds to a tephra dated at 0.75±0.06 Ma, thus also indicating an older age of the sequence. A similar situation is observed for a tephra found in drill cores from Salar de Uyuni, where the directly obtained biotite $^{40}Ar/^{39}Ar$ age of the tephra is in conflict with a younger age derived from the U-series and ^{14}C-based age model of the succession (Fornari et al., 2001; Fritz et al., 2004). Overall, the uncertainties and inconsistencies between the different dating approaches make a chronological differentiation between all available ages only of a tentative nature and suggest the need for additional criteria (e.g., other dating methods, geochemical fingerprinting) for a robust separation into different eruptive events.

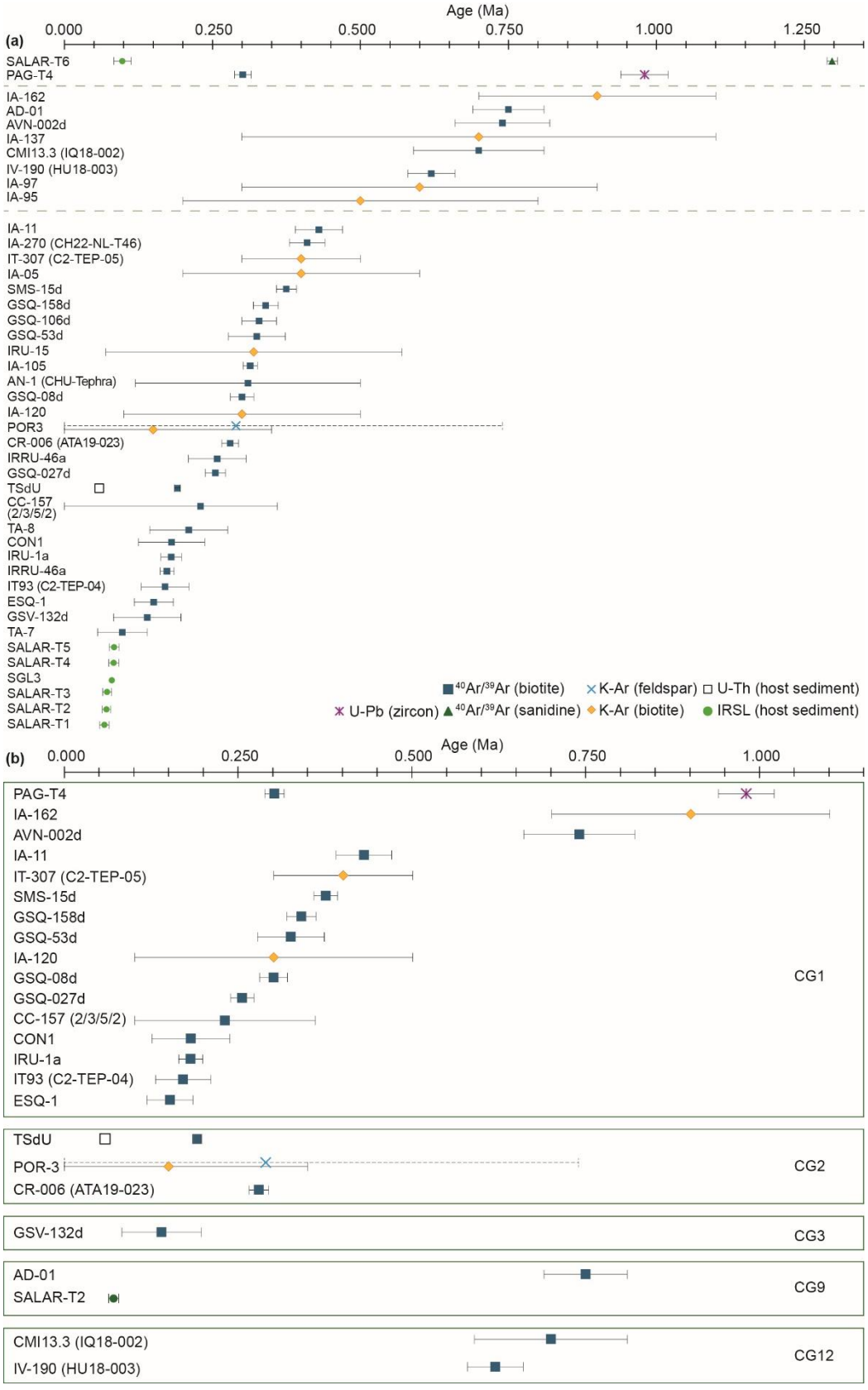

Figure 2: (a) Compilation of available chronological information for the samples of the Pleistocene being currently available within TephAta. For the references of the respective ages see Table 1. (b) Result of combined chronological and geochemical information illustrating the ages available for compositional groups CG1, 2, 3, 9, and 12. The legend illustrates the different dating techniques used for the respective samples in a and b.

4.3 Geochemistry

For 79 of the 91 sites being listed within TephAta, glass geochemical compositions of tephra layers are available, which were obtained from 82 of the 106 samples. Sixty-five of these samples were geochemically characterized for the first time and 15 samples had been characterized within the scope of previous projects within the CRC (May et al., 2020; Medialdea et al., 2020; Ritter et al., 2022). In addition, EPMA-WDS legacy data and new measurements are available for two samples (2/3/5/2, AD-01; Placzek et al., 2009; Breitkreuz et al., 2014), whereas TephAta only includes the new data. Comparing the legacy data with the respective new EPMA-WDS analyses reveals that the major and minor glass compositions of AD-01 are undistinguishably overlapping. However, the legacy data of sample 2/3/5/2 has significantly higher SiO_2 values (79.25-81.22 wt.%) compared with its reanalysis data (74.40-77.93 wt.% SiO_2), which results also in differences observed for the other element concentrations. A significant alkali loss and a SiO_2-enrichment were already noted in Breitkreuz et al. (2014), but the reason for such could not be explained. With regard to the high SiO_2 concentrations of the 2/3/5/2 legacy data, similarly high values were not observed for other samples within TephAta. Since no secondary reference data are given in the original article, a technical issue cannot be excluded

Major and minor element compositions of the samples allow a general classification of their composition based on the Total Alkali versus Silica diagram (TAS, Le Bas et al., 1986) suggesting that all samples are dominated by glass shards with rhyolitic compositions (Fig. 3). Five of these samples (SGL3, IRRU13, PAG17 ID4, ID14, ID24) have a more heterogeneous composition including also less evolved trachyandesitic, trachytic and/or dacitic shards. The samples of rhyolitic compositions exhibit silica concentrations which suggests a subdivision into three silica-types: type I (n=66) includes samples dominated by shards with silica concentrations between ~76-79 SiO_2 wt.%, type II (n=7) between ~ 73-76 SiO_2 wt.% and type III (n=9) represents a mix of both types having less homogenous rhyolitic compositions. This classification is also seen within the other major and minor element data of the samples investigated, as samples of the same silica type have very similar, partly overlapping major and minor oxide compositions (Fig. 3). The majority of the rhyolitic type I samples have a similar major and minor element geochemical composition and cannot be further separated into different geochemical clusters. Some samples of type I, however, show specific variations in TiO_2, $FeO_{(TOT)}$, CaO, K_2O and/or Na_2O concentrations, which suggest a division into several clusters (Fig. 3b, d, g-i). Tephra samples of type II and type III cannot be further separated into compositional clusters based on their major element glass geochemistry, except for individual differences observed within the CaO content (Fig. 3d,e; e.g., SALAR T4, SG17/002, TJ09-PdT CH18-T3, CH18-T5).

Due to their generally more incompatible behaviour and lower concentrations of trace elements compared to major and minor elements within the melt, trace elements effectively amplify compositional variations driven by differences in the parental magma source and magmatic history (e.g. fractional crystallization, degree and depth of melting, or residual mineral assemblages). Thus, trace element geochemistry of glass shards have been shown to be a reliable parameter for distinguishing between eruptions with similar major element composition (Tomlinson et al., 2012; Pearce, 2014; Hopkins et al., 2021).

For better differentiation among the identified geochemical clusters and to identify potential additional compositional differences, trace element data of 59 samples were considered. The individual samples show a mostly homogenous composition or indicate geochemical trends supporting that samples represent primary deposits and not a mixture of different eruptions. Trace-element concentrations normalized to values of the primitive mantle (pyrolite; Mcdonough and Sun, 1995) reveal for all samples (Fig. 4a-c) a relative enrichment of large-ion lithophile elements (LILE: Rb, Ba, Pb) against high field strength elements (HFSE: Ta, Nb, Hf, Zr), and among the latter an enrichment of light REE (LREE) compared to heavy REE (HREE), which is a pattern typical for the geodynamic continental arc setting. Combining the major, minor and trace element data enables the definition of 16 clusters, which are shortly discussed below and are listed in Table 2.

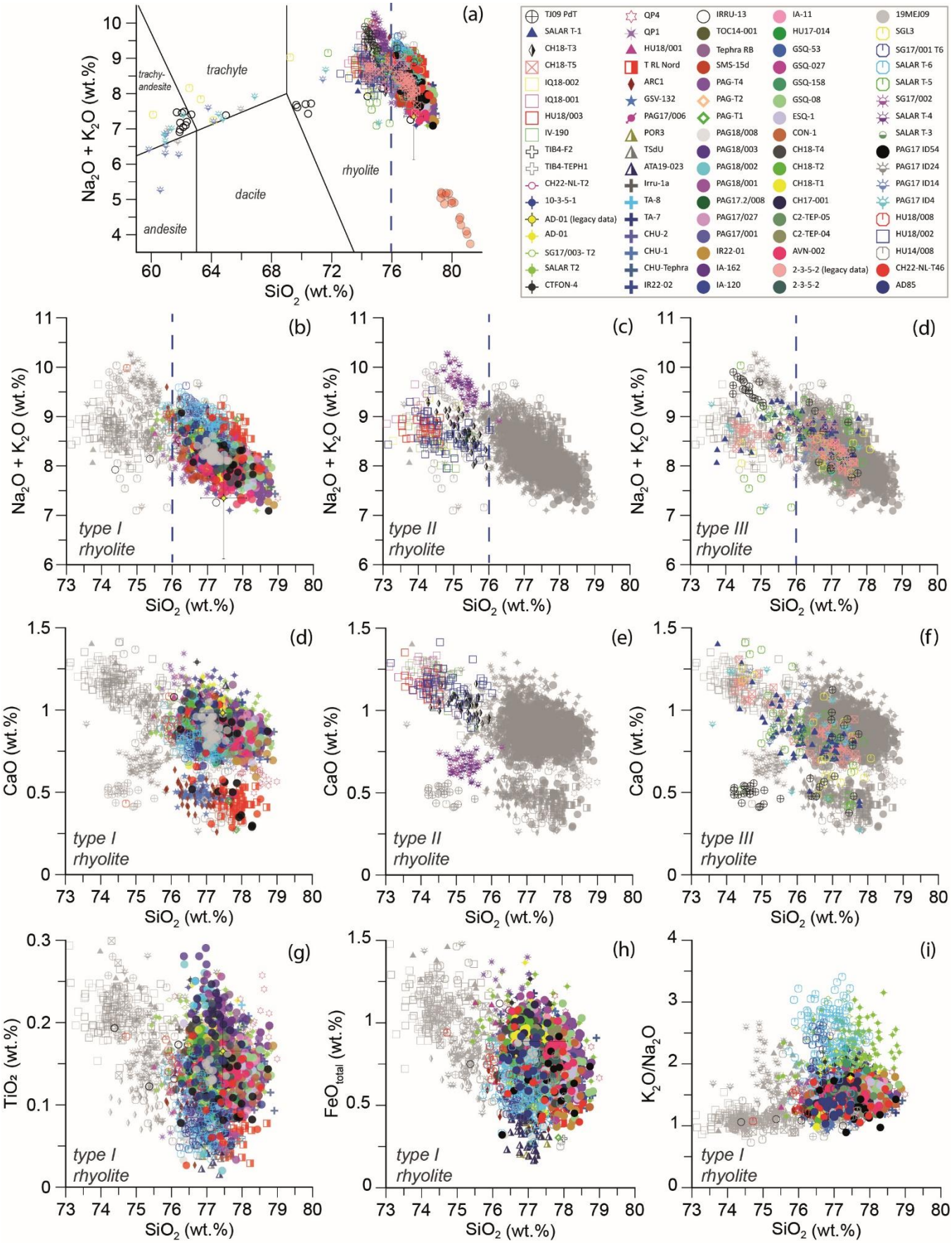

Figure 3: Geochemical classification and differentiation based on major and minor element glass compositions of the investigated tephra layers. (a) TAS-classification of all samples according to Le Bas et al. (1986). (b-c) TAS-diagram extraction for differentiation between type I, II and III rhyolites according to their silica content. (d, g-i) x-y oxide plots indicating a differentiation of type I rhyolites according to differences in the CaO, TiO_2, FeOtotal compositions (wt.%) and Na_2O/K_2O alkali-ratio. (d,e) x-y oxide plots indicating internal differentiation of type II and III rhyolites according to differences in the CaO (wt.%) composition of respective samples.

Among the 52 individual trace-element data sets of type I rhyolites, a differentiation into 11 different clusters is suggested due to distinct differences in their trace-element compositions (Fig. 4). Among them, 35 samples have a homogenous overlapping composition and are grouped in compositional group (CG) 1. CG2 comprises four samples of which three are compositionally identical (CG2.1), whereas one sample shows a generally similar pattern, although with differences in composition (CG2.2). All samples can be clearly distinguished from the other CGs by their lower HFSE and REE concentrations (Fig. 4a-c). Compositional groups 3, 4, 5, 6, 7, and 8 include one sample each, which all differ among each other (Fig. 4a-c, f-i). CG3 tephra has low Th concentrations (5-10 ppm) and a certain enrichment in HFSE (Y, Nb) and HREE compared with the other type I rhyolites, which is also observed for CG4. A characteristic depletion in Sr and Ba accompanied by elevated HFSE (except for Zr, Hf) and HREE separate CG5 from the other clusters. CG6 has slightly enriched Ba concentrations as well as HFSE and LREE, if compared to CG1. CG7 and CG8 both have a wider range of composition and have slightly lower LILE, but higher HFSE and (H+L)REE concentrations. CG9 includes four different tephra samples with a common composition, having generally higher Th concentrations (25-40 ppm, compared to 15-26 ppm of CG1), and further differ e.g. from CG1 by higher HFSE (Y, Nb, U) and LREE (La, Ce, Pr, Nd). CG10 has, relative to other rhyolite I tephra, lower Sr and Ba, but elevated HFSE (Y, Nb, Ta, U) and HREE concentrations, similar to tephra composition of CG11.

The individual trace element compositions of type II rhyolites (n=3) overlap, such as their major-element compositions, and thus are grouped as CG12. Their trace element compositions clearly differ from those of the other rhyolites (type I+III) as seen e.g., in lower LILE (expect for Ba, Sr) and higher HREE. Trace-element compositions of type III rhyolites (n=4) are heterogeneous among each other and allow a differentiation into four individual clusters (CG13, 14, 15, 16). CG13 has low HFSE and REE concentrations relative to other type III rhyolites. CG14 and CG15 are slightly similar and partially overlap with CG12. However, they clearly differ in lower HFSE (Zr, Hf), higher U concentrations, lower HFSE (Zr, U), and higher Ba concentrations.

Table 2: Overview of samples and their classification based on the Total Alkali vs. Silica composition (TAS; Le Bas et al., 1986), their assignment into rhyolites types I-III, and trace element compositional groups (TE-CG). If no trace element compositions were available, samples are listed at the end of each respective rhyolitic type. Samples which have not been geochemically investigated are listed at the bottom of the table.

TAS Group	CG-TE	samples				
rhyolite "type I"	1	19MEJ09	2/3/5/2	AVN-002d	C2-TEP-04	C2-TEP-05
		CH17-001	CH18-T1	CH18-T2	CH18-T4	CON-1
		ESQ-1	GSQ-027d	GSQ-08d	GSQ-158d	GSQ-53d
		HU17-014	IA-11	IA-120	IA-162	IR22-001
		IR22-002	IRU-1a	PAG17.2-008	PAG17/001	PAG17/027
		PAG18/001	PAG18/002	PAG18/003	PAG18/008	PAG-T1
		PAG-T2	PAG-T4	SMS-15d	Tephra RB	TOC14/001
	2.1	POR 3	TSdU	ATA19-023		
	2.2	PAG17/006				
	3	GSV-132				
	4	ARC1				
	5	Tephra RL N				
	6	HU18/001				
	7	QP1				
	8	QP4				
	9	10-3-5-1	AD-01	CTFON-4	SALAR T2	
	10	CH22-NL-T2				
	11	TIB4-Teph1	TIB4-F2			
	not analyzed	AD-85	CH22-NL-T46	HU14-008	HU18-008	PAG17 ID54
		SALAR T6	SG17/001	SG17/003	IRRU-13	CHU Tephra
		CHU-1	CHU-2	TA-7	TA-8	
rhyolite "type II"	12	IQ18-001	IQ18-002	IV-190		
	not analyzed	HU18/002	HU18/003	SALAR T4	SG17/002	
rhyolite "type III"	13	CH18-T5				
	15	SALAR T1				
	14	CH18-T3				
	16	TJ09-PdT1				
	not analyzed	PAG17 ID4	PAG17 ID14	PAG17 ID24	SALAR T5	SGL3
not analyzed	*not analyzed*	19MEJ10	23MEJ1	AN1	CC157	CH22-NL-T1
		CH22-NL-T3-1	CH22-NL-T3-2	CMI13.3	CR-006A	GSQ-106d
		IA-05	IA-105	IA-137	IA-270	IA-95
		IA-97	IRRU-46a	IRU-15	IS-155	IT-307
		IT-93	IV-189	L5		

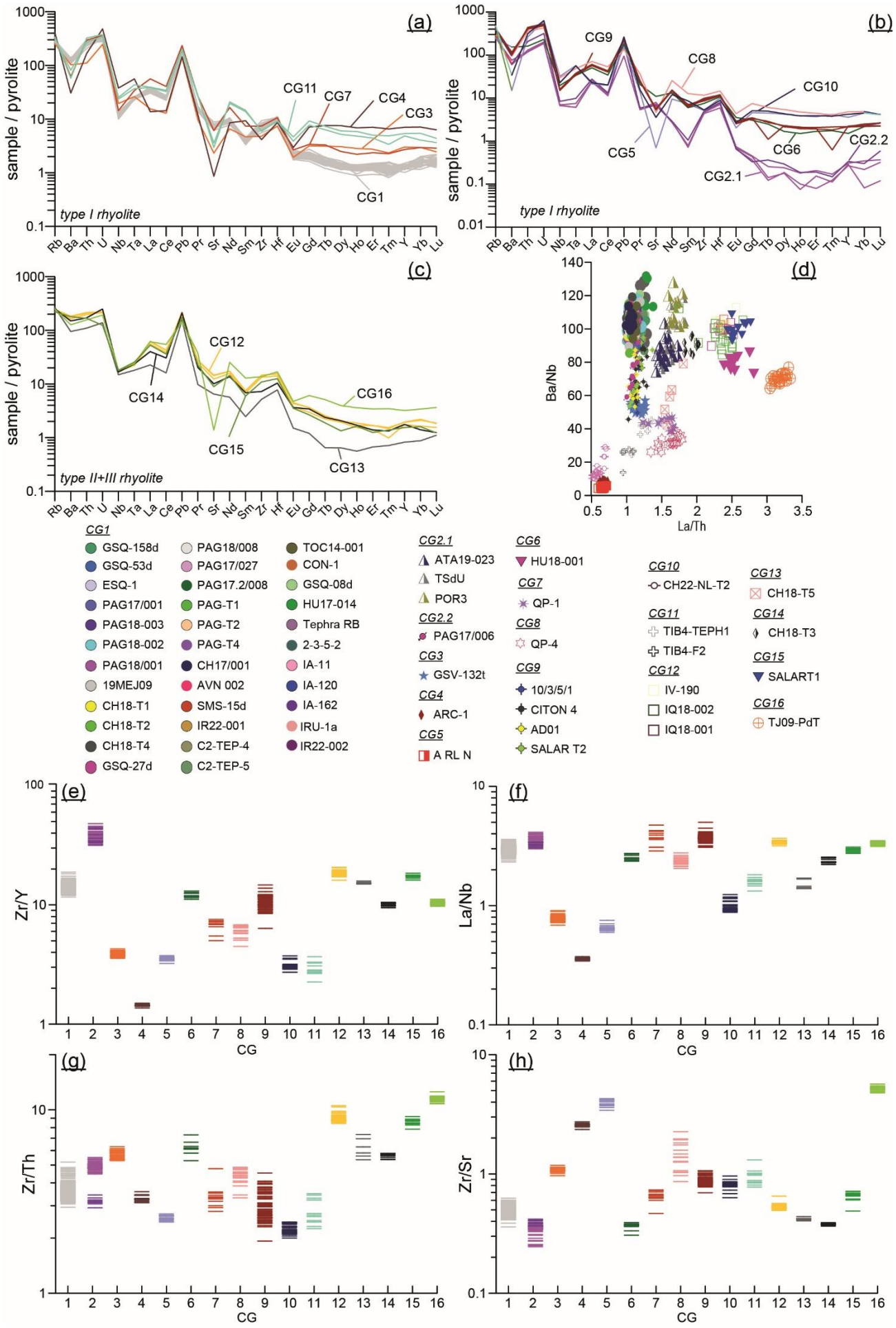

Figure 4: Geochemical classification and differentiation based on trace element glass compositions of investigated tephra layers. (a-c) Spidergrams demonstrating different degrees of enrichment/depletion of REE of the different composition groups. For each tephra sample the mean is given. Samples of the same composition group share the same color and are sorted according to their assignment to rhyolites I-III. Trace-element concentrations are normalized to values of the primitive mantle (pyrolite; Mcdonough and Sun, 1995). (d) x-y plot for trace element ratios La/Th vs. Ba/Nb to demonstrate the clustering of the different individual samples. (e-h) High-low plot of selected trace element ratios illustrating the differences between the different CG1-16. For each CG, all individual sample data are plotted as a stack.

Tephrochronological implications

The geochemical fingerprinting approach of tephra layers from the Atacama Desert enables the identification and characterization of distinct volcanic events, which promotes the investigation of inter-site tephra correlations and their spatial dispersal. A first assessment of the combined major, minor, and trace-element compositions of the tephra layers, allows a definition of 16 different geochemical clusters, which likely represent at least the same number of volcanic events. Some tephra layers were found in different sedimentary archives (e.g., tephra layers of CG1, CG2, CG9). The widespread dispersal of these tephra layers points to major eruptive events, which have the potential to be marker horizons within the sedimentary archives of the Atacama Desert. Even though for several tephra layers no correlations with other tephra deposits could be identified, their heterogenous geochemical clustering highlights their potential to contribute as geochemically distinct markers within the developing stratigraphic framework.

Although many of the investigated tephra layers have already been dated, the available chronological data often exhibit large uncertainties making it difficult to distinguish between one or multiple volcanic events. These uncertainties can be reduced by incorporating geochemical clustering results, which help to verify or challenge the proposed age distinctions and identify equivalent tephra layers derived from the same volcanic source. For 7 of the 16 geochemically defined clusters, chronological information is available and allows the assessment of 39 individual ages. Accordingly, at least 9 volcanic events have been identified for which no chronological information is available at present. As samples with ages >1 Ma have not been in the main focus of this exemplary dataset, an in-depth tephrostratigraphic evaluation of these older events is not possible to date. Overall, the available chronological and geochemical data are a valuable basis for further exploring the explosive volcanic history of the region between 22 and 1 Ma. First implications are that the geochemical fingerprinting of samples <1 Ma supports the identified bifurcation of active periods within the geochronological data and further allows characterization of individual events within the two activity periods (0.06-0.43 Ma and 0.5-0.9 Ma). For the samples >0.5 Ma, their assignment to different geochemical clusters (CG9+12) indicates at least two different eruptive events. Although their age uncertainties overlap, the combined age limits of correlated samples suggest two eruptive events at ca. 0.75 Ma (CG9) and ca. 0.6 Ma (CG12). For the remaining samples, the clustering of their geochemical data implies three potential volcanic events.

Samples belonging to CG1 (n=35) appear to be the most widespread cluster identified so far, but their available ages do not allow a distinct age constraint at present. Ages of CG1 include 14 ages with an age between 0.4-0.1 Ma, but also three ages exceeding 0.5 Ma (Fig. 2b). Their geochemically indistinguishable compositions imply a single volcanic eruption, but some samples with more precise ages within this group tentatively suggest multiple eruptions (PAG-T4, SMS-15d, GSQ-08d, GSQ-027d). Thus, it cannot be fully excluded that CG1 represents a group of repeating eruptions with identical geochemical composition that occurred in short succession. Regarding the other two identified eruptive events, no precise age can be given at present. For the older one (CG2), two differing ages of 0.191±0.005 Ma (L5/TdSU) and 0.280±0.014 Ma (ATA19-023/CR-006A) exist, whereas for the younger (CG3) only an imprecise age of 0.140±0.057 Ma (GSV-132d) is available.

In some archives, tephrochronology also provides an independent validation of direct dating of host sediment. A tephra layer (SALAR T2) of the SALAR GRANDE hillslope section (Medialdea et al., 2020) now could be correlated with a tephra layer dated in other archives, introducing an additional age of 0.75±0.06 Ma for the succession. This age, however, is in conflict with the much younger IRSL ages from the section (<0.1 Ma), but rather supports the direct age obtained for the lowermost tephra of the succession (SALAR T6: 1.297±0. 018 Ma; Medialdea et al., 2020). The distinct geochemical compositions of all tephra layers in the succession associated with different geochemical clusters supports a primary deposition of those layers and rather contradicts a reworking of the dated sanidine crystals form older material (Medialdea et al., 2020). In a sediment core recovered from Salar de Uyuni, the biotite $^{40}Ar/^{39}Ar$ age of a tephra layer (0.191±0.005 Ma; Fornari et al., 2001), is questioned by a much younger, indirect U-Th age of the host sediment (0.059 Ma; Fritz et al., 2004). This tephra layer could now be geochemically correlated with two other pyroclastic deposits being located westward of Salar de Uyuni (POR-3,

ATA19-023) and of which the age of ATA19-023 (resampled CR-006A: 0.280±0.014 Ma; Gardeweg and Sellés, 2013) is supporting also an older age. However, the large difference in their ages highlights the need for refining their chronology.

Data availability:

Table 3 lists all samples included within this manuscript and provides their IGSN number and a link to download the individual geochemical data, which is stored within TephAta (https://www.crc1211db.uni-koeln.de/tephata). In addition, the full dataset (meta and chronological data overview and geochemical data including individual major, minor and trace element glass compositions) is also made available for download at the EarthChem repository: https://doi.org/10.60520/IEDA/114209 (Leicher et al., 2026).

Table 3: Overview of samples included within the TephAta database. The sample name is given along with their IGSN and the information about which kind of data is available.

Sample	IGSN/DOI	SEM/EPMA data	LA-ICP-MS data
10-3-5-1	GF1211S-94	available	available
19MEJ09	GF1211S-4E	available	available
19MEJ10	GF1211S-4F	not available	not available
2/3/5/2	GF1211S--7	available	available
23MEJ1	GF1211S-4H	not available	not available
AD-1	GF1211S-97	available	available
AD-85	GF1211S-7X	available	not available
AN-1	GF1211S-77	not available	not available
ARC1	GF1211S-44	available	available
ATA19-023	GF1211S-3H	available	available
AVN-002d	GF1211S-33	available	available
C2-TEP-04	GF1211S--Y	available	available
C2-TEP-05	GF1211S-3-	available	available
CC-157	GF1211S-79	not available	not available
CH17-001	GF1211S-7-	available	available
CH18-T1	GF1211S-9M	available	available
CH18-T2	GF1211S-9N	available	available
CH18-T3	GF1211S-9P	available	available
CH18-T4	GF1211S-9R	available	available
CH18-T5	GF1211S-9T	available	available
CH22-NL-T1	GF1211S--C	not available	not available
CH22-NL-T2	GF1211S--E	available	available
CH22-NL-T3-1	GF1211S--F	not available	not available
CH22-NL-T3-2	GF1211S--H	not available	not available
CH22-NL-T46	GF1211S-3W	available	not available
CHU Tephra	GF1211S-34	available	not available
CHU-1	GF1211S-37	available	not available
CHU-2	GF1211S-39	available	not available
CMI13.3	GF1211S-7A	not available	not available
CON-1	GF1211S--9	available	available
CR-006A	GF1211S-7C	not available	not available
CTFON-4	GF1211S-99	available	available
ESQ-1	GF1211S--A	available	available

GSQ-027d	GF1211S-3X	available	available
GSQ-08d	GF1211S--J	available	available
GSQ-106d	GF1211S-7E	not available	not available
GSQ-158d	GF1211S--K	available	available
GSQ-53d	GF1211S--L	available	available
GSV-132d	GF1211S-3M	available	available
HU14/008	GF1211S-7Y	available	not available
HU17-014	GF1211S-9A	available	available
HU18/001	GF1211S-4U	available	available
HU18/002	GF1211S-4V	available	not available
HU18/003	GF1211S-9-	available	not available
HU18/008	GF1211S-93	available	not available
IA-05	GF1211S-7F	not available	not available
IA-105	GF1211S-7H	not available	not available
IA-11	GF1211S--M	available	available
IA-120	GF1211S--N	available	available
IA-137	GF1211S-7J	not available	not available
IA-162	GF1211S--P	available	available
IA-270	GF1211S-7K	not available	not available
IA-95	GF1211S-7L	not available	not available
IA-97	GF1211S-7M	not available	not available
IQ18-001	GF1211S-9E	available	available
IQ18-002	GF1211S-9C	available	available
IR22-001	GF1211S--T	available	available
IR22-002	GF1211S-3A	available	available
IRRU-13	GF1211S-4A	available	not available
IRRU-46a	GF1211S-7N	not available	not available
IRU-15	GF1211S-7P	not available	not available
IRU-1a	GF1211S-4C	available	available
IS-155	GF1211S-7R	not available	not available
IT-307	GF1211S-7U	not available	not available
IT-93	GF1211S-7T	not available	not available
IV-189	GF1211S-7V	not available	not available
IV-190	GF1211S-7W	available	available
L5	GF1211S-3K	not available	not available
PAG17 ID14	GF1211S-4R	available	not available
PAG17 ID24	GF1211S-4T	available	not available
PAG17 ID4	GF1211S-4P	available	not available
PAG17 ID54	GF1211S--3	available	not available
PAG17.2-008	GF1211S-4J	available	available
PAG17/001	GF1211S--U	available	available
PAG17/006	GF1211S-9F	available	available
PAG17/027	GF1211S-9H	available	available
PAG18/001	GF1211S--V	available	available
PAG18/002	GF1211S-47	available	available
PAG18/003	GF1211S-49	available	available
PAG18/008	GF1211S-9J	available	available
PAG-T1	GF1211S-9K	available	available

PAG-T2	GF1211S-9L	available	available
PAG-T4	GF1211S--4	available	available
POR 3	GF1211S-3J	available	available
QP1	GF1211S-4-	available	available
QP4	GF1211S-43	available	available
SALAR T1	GF1211S-3N	available	available
SALAR T2	GF1211S-3P	available	available
SALAR T3	GF1211S-3R	not available	not available
SALAR T4	GF1211S-3T	available	not available
SALAR T5	GF1211S-3U	available	not available
SALAR T6	GF1211S-3V	available	not available
SG17/001	GF1211S-4K	available	not available
SG17/002	GF1211S-4L	available	not available
SG17/003	GF1211S-4M	available	not available
SGL3	GF1211S-3F	available	not available
SMS-15d	GF1211S--W	available	available
TA-7	GF1211S-3C	available	not available
TA-8	GF1211S-3E	available	not available
Tephra RB	GF1211S--X	available	available
Tephra RL N	GF1211S-3Y	available	available
TIB4-F2	GF1211S-4X	available	available
TIB4-TEPH1	GF1211S-4W	available	available
TJ09-PdT1	GF1211S-4N	available	available
TOC14/001	GF1211S--R	available	available
TSdU	GF1211S-3L	available	available

Conclusions

TephAta represents a new platform to support the development of a comprehensive tephrochronological framework for the Atacama Desert in northern Chile. Its structure is strongly aligned with scientific tephra guidelines (Wallace et al., 2022) providing a centralized online repository for tephra related data. As the first platform of its kind to integrate geochemical, geochronological, and detailed outcrop metadata, TephAta preserves both new and legacy datasets to maximize data reusability. Due to the automatic implementation of IGSNs, samples become citable and have a unique identification, facilitating interoperability with global repositories. At present the dataset contains information from 106 tephra samples. For samples listed with an incomplete or missing geochemical characterization, the pending major, minor, and/or trace element analyses data will be complemented within the successive analytical work of the CRC1211. Future expansions will progressively incorporate over 400 additional samples from SERNAGEOMIN and current CRC activities. This set of samples will cover a time interval from the Early Miocene to the Holocene and has a spatial extent from the Chilean coast to the Andes along 18-30°S.

Based on the initial datasets compiled in TephAta, several data-specific insights emerge. The integrity of sample and site metadata reveals that field notes and laboratory documentation currently vary widely in detail and often lack key information, likely because many samples were not originally collected with tephrostratigraphic objectives in mind. The standardized structure provided by TephAta, in combination with dedicated field-support tools (such as sample-report templates, and app-based logging platforms like StraboSpot) will streamline and strengthen future documentation and data archiving. This improved framework will also support consistent public reporting of analytical information that aligns with best-practice metadata standards established by the global tephra research community.

In this study, most tephra layers have rhyolitic glass compositions. While major- and minor-element glass data compositions distinguish only a subset of tephra layers, trace-element glass compositions provide the most robust means of differentiation. Based on these geochemical differences, at least 16 distinct eruptive events have been identified, allowing for potential regional correlations. Despite these advances, the uncertainties in existing geochronological data require careful reassessment. Existing ages should be supported by additional, higher precision dating, before used as tephrochronological tie points. Implementing methods such as zircon double-dating (Danišík et al., 2017), will help to account for pre-eruptive mineral histories and improve discrimination among tephra layers of similar age and geochemical composition. Furthermore, obtaining new chronological data for the numerous identified eruptive events (CG1, 4-8, 10, 11, 13-16), is essential to strengthening the tephrochronological framework and overcoming the inherent dating challenges of arid environments.

Overall, this initial dataset demonstrates the value and potential of a tephrochronological database for the region. It also highlights that establishing a robust regional tephrochronological framework requires a large set of samples with adequate spatial and temporal coverage. This includes the tephrochronological characterization of proximal major eruptive products to link widespread distal tephra layers with their volcanic sources. As the database grows, it will enhance our understanding of the Andean volcanic history, particularly in a region where distal archives play a key role in unraveling eruptive sequences, as demonstrated elsewhere. (Schindlbeck et al., 2018; Leicher et al., 2023; Vineberg et al., 2024). In addition, the individual geochemical data for the tephra samples offer valuable opportunities to investigate magmatic processes, such as the varying degrees of element depletion and enrichment of characteristic elements observed in this dataset.

Supplement:

Supplementary Material

Supplementary Figures S1-S8: Overview of input masks for the seven different categories (Site, Sample, Physical Properties, Geochemistry, Chronology, Chronostratigraphy, Tephra Correlation Group) of the TephAta database.

A list of all input fields and their brief description is given in Supplementary Table S1. A list of all dropdown options is given in Supplementary Table S2.

Supplementary Table S1:

Overview table of input fields within TephAta. For each input option within TephAta, the respective field name is given along with its overall category (e.g., “site” or “geochemistry”), the field type (e.g., text, dropdown selection, or data upload) and a short explanation of the respective field.

Supplementary Table S2:

The table contains all dropdown options within the TephAta database, organized by their respective categories and input fields.

Author contribution

Conceptualization: NL, VW, BW, GB

Data curation: NL, VF

Funding acquisition, Supervision: VW, BW, GB

Resources: AQJ, PVI, FSV, GG, CB, AS, DG, LC, IRA

Software: VF, TK

Investigation, Validation, Methodology: NL, VW, FW, ML, KK

Writing (original draft preparation), Visualization: NL

Writing (review and editing): all authors

Competing interests: The authors declare that they have no conflict of interest.

Acknowledgement

This research has been supported by the German Research Foundation (DFG) as part of Collaborative Research Centre (CRC) 1211 "Earth – Evolution at the Dry Limit", sub-project D06, A02 and Z03 (grant nos. SFB 1211/2 2020. SFB1211/3 2024). AQ, PV, FS received funding of the National Mapping Program of the SERNAGEOMIN. Gerhard Wörner, Jay Quade, Theresa Jordan, Felipe Aguilera Barraza, and Susana Layana are gratefully acknowledged for sharing sample material. Chong, G., and Jensen A. (Universidad Católica del Norte, Antofagasta) supported AS and LC during sampling. Furthermore, all (associated) CRC members who contributed sample material or assisted during field work are recognized. Reiner Kleinschrodt, Yannick Bussweiler and Hanna Cieszynski are thanked for providing access to and supporting the use of the EPMA-WDS and SEM-EDS at the University of Cologne. We sincerely thank the reviewers for their thoughtful and constructive feedback, which has significantly improved the quality of the manuscript.

References

Abbott, P. M., Griggs, A. J., Bourne, A. J., Chapman, M. R., and Davies, S. M.: Tracing marine cryptotephras in the North Atlantic during the last glacial period: Improving the North Atlantic marine tephrostratigraphic framework, Quat. Sci. Rev., 189, 169-186, https://doi.org/10.1016/j.quascirev.2018.03.023, 2018.

Albert, P. G., Smith, V. C., Suzuki, T., McLean, D., Tomlinson, E. L., Miyabuchi, Y., Kitaba, I., Mark, D. F., Moriwaki, H., Nakagawa, T., and Members, S. P.: Geochemical characterisation of the Late Quaternary widespread Japanese tephrostratigraphic markers and correlations to the Lake Suigetsu sedimentary archive (SG06 core), Quat. Geochronol., 52, 103-131, https://doi.org/10.1016/j.quageo.2019.01.005, 2019.

Allmendinger, R. W., Jordan, T. E., Kay, S. M., and Isacks, B. L.: The evolution of the Altiplano-Puna plateau of the Central Andes, Annu. Rev. Earth Planet. Sci., 25, 139-174, https://doi.org/10.1146/annurev.earth.25.1.139, 1997.

Astudillo, N., Ferrando, R., Montecino, D., Espinoza, F., Venegas, C., Matthews, S., Cornejo, P., and Arévalo, C.: Carta Augusta Victoria, región de Antofagasta, Servicio Nacional de Geología y Minería, Carta Geológica de Chile, Serie Geología Básica, 189, Santiago, Chile, 97 p., ISSN:0717-7283 Inscripción No. 285.185, 2017.

Blanco, N. and Tomlinson, A.: Carta Guatacondo, región de Tarapacá, Servicio Nacional de Geología y Minería, Carta Geológica de Chile, Serie Geología Básica, 156, Santiago, Chile, 116 p., ISSN:0717-7283 Inscripción No. 235.690, 2013.

Brandmeier, M. and Wörner, G.: Compositional variations of ignimbrite magmas in the Central Andes over the past 26 Ma — A multivariate statistical perspective, Lithos, 262, 713-728, https://doi.org/10.1016/j.lithos.2016.07.011, 2016.

Breitkreuz, C., de Silva, S. L., Wilke, H. G., Pfänder, J. A., and Renno, A. D.: Neogene to Quaternary ash deposits in the Coastal Cordillera in northern Chile: Distal ashes from supereruptions in the Central Andes, J. Volcanol. Geotherm. Res., 269, 68-82, https://doi.org/10.1016/j.jvolgeores.2013.11.001, 2014.

Bronk Ramsey, C., Housley, R. A., Lane, C. S., Smith, V. C., and Pollard, A. M.: The RESET tephra database and associated analytical tools, Quat. Sci. Rev., 118, 33-47, https://doi.org/10.1016/j.quascirev.2014.11.008, 2015.

Burns, D. H. and de Silva, S. L.: Andesites and evolution of the continental crust: Perspectives from the Central Volcanic Zone of the Andes, Front. Earth Sci., 10, https://doi.org/10.3389/feart.2022.961130, 2023.

Burns, D. H., de Silva, S. L., Tepley, F., Schmitt, A. K., and Loewen, M. W.: Recording the transition from flare-up to steady-state arc magmatism at the Purico-Chascon volcanic complex, northern Chile, Earth Planet. Sci. Lett., 422, 75-86, https://doi.org/10.1016/j.epsl.2015.04.002, 2015.

Cameron, C. E., Crass, S. W., and Staff, A.: Geologic database of information on volcanoes in Alaska (GeoDIVA), DDS, 20, https://doi.org/10.14509/30901, 2022.

Carrizo, D., González, G., and Dunai, T.: Constricción neógena en la Cordillera de la Costa, norte de Chile: neotectónica y datación de superficies con 21Ne cosmogónico, Rev. Geol. Chile, 35, 01-38, http://dx.doi.org/10.4067/S0716-02082008000100001, 2008.

CRC1211DB-TephAta: https://www.crc1211db.uni-koeln.de/tephata/, last access: 16 March 2026.

Danišík, M., Schmitt, A. K., Stockli, D. F., Lovera, O. M., Dunkl, I., and Evans, N. J.: Application of combined U-Th-disequilibrium/U-Pb and (U-Th)/He zircon dating to tephrochronology, Quat. Geochronol., 40, 23-32, https://doi.org/10.1016/j.quageo.2016.07.005, 2017.

de Silva, S. L.: Geochronology and stratigraphy of the ignimbrites from the 21°30′S to 23°30′S portion of the Central Andes of northern Chile, J. Volcanol. Geotherm. Res., 37, 93-131, https://doi.org/10.1016/0377-0273(89)90065-6, 1989a.

de Silva, S. L.: Altiplano-Puna volcanic complex of the central Andes, Geology, 17, 1102-1106, https://doi.org/10.1130/0091-7613(1989)017%3C1102:APVCOT%3E2.3.CO;2, 1989b.

de Silva, S. L. and Kay, S. M.: Turning up the Heat: High-Flux Magmatism in the Central Andes, Elements, 14, 245-250, https://doi.org/10.2138/gselements.14.4.245, 2018.

Dunai, T. J., González López, G. A., and Juez-Larré, J.: Oligocene-Miocene age of aridity in the Atacama Desert revealed by exposure dating of erosion-sensitive landforms, Geology, 33, 321-324, https://doi.org/10.1130/G21184.1, 2005.

Dunai, T. J., Melles, M., Quandt, D., Knief, C., and Amelung, W.: Whitepaper: Earth – Evolution at the dry limit, Global Planet. Change, 193, 103275, https://doi.org/10.1016/j.gloplacha.2020.103275, 2020.

Escribano, A., Martínez, E., Domagala, J. P., Padel, M., Espinoza, V., Jorquera, B., Contreras, F., Pablo, J., De La Cruz, S., and Calderón, N.: Cartas Bahía Isla Blanca y Taltal, región de Antofagasta Servicio Nacional de Geología y Minería, Carta Geológica de Chile, Serie Geología Básica 164-165, Santiago, Chile, 75 p., ISSN:0717-7283 Inscripción No. 235.124, 2013.

Evenstar, L. A., Mather, A. E., Hartley, A. J., Stuart, F. M., Sparks, R. S. J., and Cooper, F. J.: Geomorphology on geologic timescales: Evolution of the late Cenozoic Pacific paleosurface in Northern Chile and Southern Peru, Earth Sci. Rev., 171, 1-27, https://doi.org/10.1016/j.earscirev.2017.04.004, 2017.

Feng, W., Yang, J., Bao, C., Kong, D., and Chen, M.-T.: A Millennial-Scale Tephra Event-Stratigraphic Record of the South China Sea since the Penultimate Interglacial, Lithosphere, 2022, https://doi.org/10.2113/2022/9074201, 2022.

Fornari, M., Risacher, F., and Féraud, G.: Dating of paleolakes in the central Altiplano of Bolivia, Palaeogeogr. Palaeoclimatol. Palaeoecol., 172, 269-282, https://doi.org/10.1016/S0031-0182(01)00301-7, 2001.

Fritz, S. C., Baker, P. A., Lowenstein, T. K., Seltzer, G. O., Rigsby, C. A., Dwyer, G. S., Tapia, P. M., Arnold, K. K., Ku, T. L., and Luo, S. D.: Hydrologic variation during the last 170,000 years in the southern hemisphere tropics of South America, Quat. Res., 61, 95-104, https://doi.org/10.1016/j.yqres.2003.08.007, 2004.

Gardeweg, M. and Sellés, D.: Geología del área Collacagua-Rinconada, región de Tarapacá, Servicio Nacional de Geología y Minería, Carta Geológica de Chile, Serie Geología Básica Santiago, Chile, 84 p., ISSN:0717-7283 Inscripción No. 235.793, 2013.

Gehrels, M. J., Lowe, D. J., Hazell, Z. J., and Newnham, R. M.: A continuous 5300-yr Holocene cryptotephrostratigraphic record from northern New Zealand and implications for tephrochronology and volcanic hazard assessment, The Holocene, 16, 173-187, https://doi.org/10.1191/0959683606hl918rp, 2006.

Giaccio, B., Leicher, N., Mannella, G., Monaco, L., Regattieri, E., Wagner, B., Zanchetta, G., Gaeta, M., Marra, F., Nomade, S., Palladino, D. M., Pereira, A., Scheidt, S., Sottili, G., Wonik, T., Wulf, S., Zeeden, C., Ariztegui, D., Cavinato, G. P., Dean, J. R., Florindo, F., Leng, M. J., Macrì, P., Niespolo, E., Renne, P. R., Rolf, C., Sadori, L., Thomas, C., and Tzedakis, P. C.: Extending the tephra and palaeoenvironmental record of the Central Mediterranean back to 430 ka: A new core from Fucino Basin, central Italy, Quat. Sci. Rev., 225, 106003, https://doi.org/10.1016/j.quascirev.2019.106003, 2019.

Griggs, A. J., Davies, S. M., Abbott, P. M., Rasmussen, T. L., and Palmer, A. P.: Optimising the use of marine tephrochronology in the North Atlantic: a detailed investigation of the Faroe Marine Ash Zones II, III and IV, Quat. Sci. Rev., 106, 122-139, https://doi.org/10.1016/j.quascirev.2014.04.031, 2014.

Hopkins, J. L., Bidmead, J. E., Lowe, D. J., Wysoczanski, R. J., Pillans, B. J., Ashworth, L., Rees, A. B. H., and Tuckett, F.: TephraNZ: a major- and trace-element reference dataset for glass-shard analyses from prominent Quaternary rhyolitic tephras in New Zealand and implications for correlation, GChron, 3, 465-504, https://doi.org/10.5194/gchron-3-465-2021, 2021.

Hora, J. M., Singer, B. S., Jicha, B. R., Beard, B. L., Johnson, C. M., de Silva, S., and Salisbury, M.: Volcanic biotite-sanidine 40Ar/39Ar age discordances reflect Ar partitioning and pre-eruption closure in biotite, Geology, 38, 923-926, https://doi.org/10.1130/g31064.1, 2010.

Horn, S.: Intra- und intervulkanische Variationen entlang der Zentralen Vulkanzone in Nordchile (17-22 °S): · Petrographische und geochemische Untersuchungen, Diploma thesis, Institut für Geowissenschaften, Johannes Gutenberg Universität Mainz, Mainz, 168 pp., 1991.

Jochum, K. P., Weis, U., Stoll, B., Kuzmin, D., Yang, Q. C., Raczek, I., Jacob, D. E., Stracke, A., Birbaum, K., Frick, D. A., Gunther, D., and Enzweiler, J.: Determination of Reference Values for NIST SRM 610-617 Glasses Following ISO Guidelines, Geostand. Geoanal. Res., 35, 397-429, https://doi.org/10.1111/j.1751-908X.2011.00120.x, 2011.

Jochum, K. P., Stoll, B., Herwig, K., Willbold, M., Hofmann, A. W., Amini, M., Aarburg, S., Abouchami, W., Hellebrand, E., Mocek, B., Raczek, I., Stracke, A., Alard, O., Bouman, C., Becker, S., Ducking, M., Bratz, H., Klemd, R., de Bruin, D., Canil, D., Cornell, D., de Hoog, C. J., Dalpe, C., Danyushevsky, L., Eisenhauer, A., Gao, Y. J., Snow, J. E., Goschopf, N., Gunther, D., Latkoczy, C., Guillong, M., Hauri, E. H., Hofer, H. E., Lahaye, Y., Horz, K., Jacob, D. E., Kassemann, S. A., Kent, A. J. R., Ludwig, T., Zack, T., Mason, P. R. D., Meixner, A., Rosner, M., Misawa, K. J., Nash, B. P., Pfander, J., Premo, W. R., Sun, W. D., Tiepolo, M., Vannucci, R., Vennemann, T., Wayne, D.,

and Woodhead, J. D.: MPI-DING reference glasses for in situ microanalysis: New reference values for element concentrations and isotope ratios, Geochem. Geophys. Geosyst, 7, 1525-2027, https://doi.org/10.1029/2005gc001060, 2006.

Jordan, T. E., Kirk-Lawlor, N. E., Blanco, N., Rech, J. A., and Cosentino, N. J.: Landscape modification in response to repeated onset of hyperarid paleoclimate states since 14 Ma, Atacama Desert, Chile, Geol. Soc. Am. Bull., 126, 1016-1046, https://doi.org/10.1130/B30978.1, 2014.

Kay, S. M., Coira, B. L., Caffe, P. J., and Chen, C. H.: Regional chemical diversity, crustal and mantle sources and evolution of central Andean Puna plateau ignimbrites, J. Volcanol. Geotherm. Res., 198, 81-111, https://doi.org/10.1016/j.jvolgeores.2010.08.013, 2010.

Kern, J. M., de Silva, S. L., Schmitt, A. K., Kaiser, J. F., Iriarte, A. R., and Economos, R.: Geochronological imaging of an episodically constructed subvolcanic batholith: U-Pb in zircon chronochemistry of the Altiplano-Puna Volcanic Complex of the Central Andes, Geosphere, 12, 1054-1077, https://doi.org/10.1130/ges01258.1, 2016.

Kirk-Lawlor, N. E., Jordan, T. E., Rech, J. A., and Lehmann, S. B.: Late Miocene to Early Pliocene paleohydrology and landscape evolution of Northern Chile, 19° to 20° S, Palaeogeogr. Palaeoclimatol. Palaeoecol., 387, 76-90, https://doi.org/10.1016/j.palaeo.2013.07.011, 2013.

Koppers, A. A. P.: ArArCALC—software for 40Ar/39Ar age calculations, Comput. Geosci., 28, 605-619, https://doi.org/10.1016/S0098-3004(01)00095-4, 2002.

Kuehn, S., Bursik, M., Kurbatov, A., Lehnert, K., Loewen, M., Profeta, L., Ramdeen, S., and Wallace, K.: Tephra Community Tools for Archiving Sample Information, Analytical Methods, Samples Geochemistry, and Standards Geochemistry at SESAR and EarthChem, Microsc. Microanal., 29, 242-242, https://doi.org/10.1093/micmic/ozad067.108, 2023.

Kuiper, K. F., Deino, A., Hilgen, F. J., Krijgsman, W., Renne, P. R., and Wijbrans, J. R.: Synchronizing Rock Clocks of Earth History, Science, 320, 500-504, https://doi.org/10.1126/science.1154339, 2008.

Kurbatov, A., Dunbar, N. W., Iverson, N. A., Gerbi, C. C., Yates, M. G., Kalteyer, D., and McIntosh, W. C.: Antarctic Tephra Database (AntT) AGU Fall Meeting 2014, San Francisco, 15-19 December 2014, V31C-4760, 2014.

Kutterolf, S., Schindlbeck, J. C., Anselmetti, F. S., Ariztegui, D., Brenner, M., Curtis, J., Schmid, D., Hodell, D. A., Mueller, A., Pérez, L., Pérez, W., Schwalb, A., Frische, M., and Wang, K. L.: A 400-ka tephrochronological framework for Central America from Lake Petén Itzá (Guatemala) sediments, Quat. Sci. Rev., 150, 200-220, https://doi.org/10.1016/j.quascirev.2016.08.023, 2016.

Le Bas, M. J. L., Maitre, R. W. L., Streckeisen, A., and Zanettin, B.: A Chemical Classification of Volcanic Rocks Based on the Total Alkali-Silica Diagram, J. Petrol., 27, 745-750, https://doi.org/10.1093/petrology/27.3.745, 1986.

Lee, J. Y., Marti, K., Severinghaus, J. P., Kawamura, K., Yoo, H. S., Lee, J. B., and Kim, J. S.: A redetermination of the isotopic abundances of atmospheric Ar, Geochim. Cosmochim. Acta, 70, 4507-4512, https://doi.org/10.1016/j.gca.2006.06.1563, 2006.

Leicher, N.: EPMA-WDS settings for glass at University of Cologne - v1, Interdisciplinary Earth Data Alliance (IEDA) [dataset], https://doi.org/10.26022/IEDA/111986, 2021.

Leicher, N. and Lagos, M.: LA-ICP-MS at University of Bonn - v1, Interdisciplinary Earth Data Alliance (IEDA) [dataset], https://doi.org/10.26022/IEDA/111989, 2021.

Leicher, N., Giaccio, B., Zanchetta, G., Sulpizio, R., Albert, P. G., Tomlinson, E. L., Lagos, M., Francke, A., and Wagner, B.: Lake Ohrid's tephrochronological dataset reveals 1.36 Ma of Mediterranean explosive volcanic activity, Sci. Data, 8, 231, https://doi.org/10.1038/s41597-021-01013-7, 2021.

Leicher, N., Monaco, L., Giaccio, B., Nomade, S., Pereira, A., Mannella, G., Wulf, S., Sottili, G., Palladino, D. M., Zanchetta, G., and Wagner, B.: Central Mediterranean tephrochronology for the time interval 250–315 ka derived from the Fucino sediment succession, Boreas, 53, 164-185, https://doi.org/10.1111/bor.12637, 2023.

Leicher N., W. V., Wombacher F., Lagos, M.: Tephrostratigraphic and tephrochonological dataset of tephra layers from northern Chile, Version 1.0, Interdisciplinary Earth Data Alliance (IEDA) [dataset], https://doi.org/10.60520/IEDA/114209, 2026.

Lowe, D. J.: Tephrochronology and its application: A review, Quat. Geochronol., 6, 107-153, https://doi.org/10.1016/j.quageo.2010.08.003, 2011.

Lowe, D. J., Blaauw, M., Hogg, A. G., and Newnham, R. M.: Ages of 24 widespread tephras erupted since 30,000 years ago in New Zealand, with re-evaluation of the timing and palaeoclimatic implications of the Lateglacial cool episode recorded at Kaipo bog, Quat. Sci. Rev., 74, 170-194, https://doi.org/10.1016/j.quascirev.2012.11.022, 2013.

Lowe, D. J., Pearce, N. J. G., Jorgensen, M. A., Kuehn, S. C., Tryon, C. A., and Hayward, C. L.: Correlating tephras and cryptotephras using glass compositional analyses and numerical and statistical methods: Review and evaluation, Quat. Sci. Rev., 175, 1-44, https://doi.org/10.1016/j.quascirev.2017.08.003, 2017.

Lowe, J. J., Ramsey, C. B., Housley, R. A., Lane, C. S., and Tomlinson, E. L.: The RESET project: constructing a European tephra lattice for refined synchronisation of environmental and archaeological events during the last c. 100 ka, Quat. Sci. Rev., 118, 1-17, https://doi.org/10.1016/j.quascirev.2015.04.006, 2015.

Mamani, M., Wörner, G., and Sempere, T.: Geochemical variations in igneous rocks of the Central Andean orocline (13°S to 18°S): Tracing crustal thickening and magma generation through time and space, Geol. Soc. Am. Bull., 122, 162-182, https://doi.org/10.1130/B26538.1, 2010.

Mana, S. and DiMaggio, E.: Broadening Access To Volcanic Datasets From East Africa, Connects 2023, Pittsburgh, Pennsylvania, USA, 15-18 October 2023, 2023AM-393916, https://doi.org/10.1130/abs/2023AM-393916, 2023.

Marinovic, N., Smoje, I., Maksaev, V., Herve, M., and Mpodozis, C.: Hoja Aguas Blancas, Servicio Nacional de Geología y Minería, Carta Geológica de Chile, Serie Geología Básica 70, Santiago, Chile, 150 p., ISSN:0716-7555 Inscripción No. 81271, 1995.

Marquardt, C., Fornari, M., Lavenu, A., Easton, G., Ortlieb, L., Ritz, J.-F., and Philip, H.: Volcanic ash dating from the Mejillones Peninsula (23ºS): Implications for the Neogene outer fore-arc stratigraphy, tectonics and volcanic relationships, 6th International Symposium on Andean Geodynamics, Barcelona, 12-14 September 2005, Extended Abstracts: 477-480, 2005.

Martínez Fontaine, C., Peña-Araya, V., Marmo, C., Le Morvan, M., Delpech, G., Fontijn, K., Siani, G., and Cosyn-Wexsteen, L.: BOOM! Tephrochronological dataset and exploration tool of the Southern (33–46° S) and Austral (49–55° S) volcanic zones of the Andes, Quat. Sci. Rev., 316, 108254, https://doi.org/10.1016/j.quascirev.2023.108254, 2023.

May, S. M., Meine, L., Hoffmeister, D., Brill, D., Medialdea, A., Wennrich, V., Gröbner, M., Schulte, P., Steininger, F., Deprez, M., de Kock, T., and Bubenzer, O.: Origin and timing of past hillslope activity in the hyper-arid core of the Atacama Desert – The formation of fine sediment lobes along the Chuculay Fault System, Northern Chile, Global Planet. Change, 184, 103057, https://doi.org/10.1016/j.gloplacha.2019.103057, 2020.

McDonough, W. F. and Sun, S. s.: The composition of the Earth, Chem. Geol., 120, 223-253, https://doi.org/10.1016/0009-2541(94)00140-4, 1995.

Medialdea, A., May, S. M., Brill, D., King, G., Ritter, B., Wennrich, V., Bartz, M., Zander, A., Kuiper, K., Hurtado, S., Hoffmeister, D., Schulte, P., Gröbner, M., Opitz, S., Brückner, H., and Bubenzer, O.: Identification of humid periods in the Atacama Desert through hillslope activity established by infrared stimulated luminescence (IRSL) dating, Global Planet. Change, 185, 103086, https://doi.org/10.1016/j.gloplacha.2019.103086, 2020.

Medina, E., Jensen, A., Niemeyer, H., Wilke, H. G., Cembrano, J., García, M., Riquelme, R., Espinoza, S., and Chong, G.: Cartas Tocopilla y Maria Elena, región de Antofagasta, Servicio Nacional de Geología y Minería, Carta Geológica de Chile, Serie Geología Básica, 141-142, Santiago, Chile, 58 p., ISSN:0717-7283 Inscripción No. 224.403, 2012.

Min, K., Mundil, R., Renne, P. R., and Ludwig, K. R.: A test for systematic errors in 40Ar/39Ar geochronology through comparison with U/Pb analysis of a 1.1-Ga rhyolite, Geochim. Cosmochim. Acta, 64, 73-98, https://doi.org/10.1016/S0016-7037(99)00204-5, 2000.

Newton, A. J., Dugmore, A. J., and Gittings, B. M.: Tephrabase: tephrochronology and the development of a centralised European database, J. Quat. Sci., 22, 737-743, https://doi.org/10.1002/jqs.1094, 2007.

Oliveros, V., González, J., Espinoza Vargas, M., Vásquez, P., Rossel, P., Creixell, C., Sepúlveda, F., and Bastias, F.: The Early Stages of the Magmatic Arc in the Southern Central Andes, in: The Evolution of the Chilean-Argentinean Andes, edited by: Folguera, A., Contreras-Reyes, E., Heredia, N., Encinas, A., B. Iannelli, S., Oliveros, V., M. Dávila, F., Collo, G., Giambiagi, L., Maksymowicz, A., Iglesia Llanos, M. P., Turienzo, M., Naipauer, M., Orts, D., D. Litvak, V., Alvarez, O., and Arriagada, C., Springer International Publishing, Cham, 165-190, https://doi.org/10.1007/978-3-319-67774-3_7, 2018.

Paton, C., Hellstrom, J., Paul, B., Woodhead, J., and Hergt, J.: Iolite: Freeware for the visualisation and processing of mass spectrometric data, J. Anal. At. Spectrom., 26, 2508-2518, https://doi.org/10.1039/c1ja10172b, 2011.

Pearce, N. J. G.: Towards a protocol for the trace element analysis of glass from rhyolitic shards in tephra deposits by laser ablation ICP-MS, J. Quat. Sci., 29, 627-640, https://doi.org/10.1002/jqs.2727, 2014.

Phillips, D. and Matchan, E. L.: Ultra-high precision 40Ar/39Ar ages for Fish Canyon Tuff and Alder Creek Rhyolite sanidine: New dating standards required?, Geochim. Cosmochim. Acta, 121, 229-239, https://doi.org/10.1016/j.gca.2013.07.003, 2013.

Placzek, C., Quade, J., Rech, J. A., Patchett, P. J., and de Arce, C. P.: Geochemistry, chronology and stratigraphy of Neogene tuffs of the Central Andean region, Quat. Geochronol., 4, 22-36, https://doi.org/10.1016/j.quageo.2008.06.002, 2009.

Portnyagin, M. V., Ponomareva, V. V., Zelenin, E. A., Bazanova, L. I., Pevzner, M. M., Plechova, A. A., Rogozin, A. N., and Garbe-Schönberg, D.: TephraKam: geochemical database of glass compositions in tephra and welded tuffs from the Kamchatka volcanic arc (northwestern Pacific), Earth Syst. Sci. Data, 12, 469-486, https://doi.org/10.5194/essd-12-469-2020, 2020.

Quezada, A., Blanco, N., Vásquez, P., and Sepúlveda, F.: Ar-Ar (biotite) dating of deformed tephra layers (ashes) interbedded in salar Grande halite deposits, Atacama Desert, I Region, Chile, 15. Congreso Geolólogico Chileno, Cocepción, Chile, 18-23 November 2018, 15785-a, 2018.

Riede, F., Bazely, O., Newton, A. J., and Lane, C. S.: A Laacher See-eruption supplement to Tephrabase: Investigating distal tephra fallout dynamics, Quat. Int., 246, 134-144, https://doi.org/10.1016/j.quaint.2011.06.029, 2011.

Ritter, B., Stuart, F. M., Binnie, S. A., Gerdes, A., Wennrich, V., and Dunai, T. J.: Neogene fluvial landscape evolution in the hyperarid core of the Atacama Desert, Sci. Rep., 8, 13952, https://doi.org/10.1038/s41598-018-32339-9, 2018.

Ritter, B., Diederich-Leicher, J. L., Binnie, S. A., Stuart, F. M., Wennrich, V., Bolten, A., and Dunai, T. J.: Impact of CaSO(4)-rich soil on Miocene surface preservation and Quaternary sinuous to meandering channel forms in the hyperarid Atacama Desert, Sci. Rep., 12, 17951, https://doi.org/10.1038/s41598-022-22787-9, 2022.

Ritter, B., Mohren, J., Binnie, S. A., Wennrich, V., Dunkl, I., Albert, R., Gerdes, A., LoBue, S., and Dunai, T. J.: Shaping the Huara Intrusive Complex in the Hyperarid Atacama Desert-Erosional Near-Stasis Contrasting High Topographic Gradients, J. Geophys. Res.: Earth Surf., 128, e2022JF006986, https://doi.org/10.1029/2022jf006986, 2023.

Rodríguez, I., Roche, O., Moune, S., Aguilera, F., Campos, E., and Pizarro, M.: Evolution of Irruputuncu volcano, Central Andes, northern Chile, J. South Am. Earth Sci., 63, 385-399, https://doi.org/10.1016/j.jsames.2015.08.012, 2015.

Sáez, A., Cabrera, L., Jensen, A., and Chong, G.: Late Neogene lacustrine record and palaeogeography in the Quillagua–Llamara basin, Central Andean fore-arc (northern Chile), Palaeogeogr. Palaeoclimatol. Palaeoecol., 151, 5-37, https://doi.org/10.1016/S0031-0182(99)00013-9, 1999.

Sáez, A., Cabrera, L., Garcés, M., van den Bogaard, P., Jensen, A., and Gimeno, D.: The stratigraphic record of changing hyperaridity in the Atacama desert over the last 10 Ma, Earth Planet. Sci. Lett., 355, 32-38, https://doi.org/10.1016/j.epsl.2012.08.029, 2012.

Sáez, A., Hernández, A., Pimentel, A., Andrade, M., Bao, R., Raposeiro, P. M., Gonçalves, V., Benavente, M., Pla-Rabes, S., Ramalho, R., and Giralt, S.: Westerlies migrations and volcanic records over the past 4000 years from the Azores lacustrine sequences. Exploring correlations and impacts on Western Europe, Global Planet. Change, 246, 104698, https://doi.org/10.1016/j.gloplacha.2025.104698, 2025.

Sagawa, T., Nagahashi, Y., Satoguchi, Y., Holbourn, A., Itaki, T., Gallagher, S. J., Saavedra-Pellitero, M., Ikehara, K., Irino, T., and Tada, R.: Integrated tephrostratigraphy and stable isotope stratigraphy in the Japan Sea and East China Sea using IODP Sites U1426, U1427, and U1429, Expedition 346 Asian Monsoon, Prog. Earth Planet. Sci., 5, 18, https://doi.org/10.1186/s40645-018-0168-7, 2018.

Salisbury, M. J., Jicha, B. R., de Silva, S. L., Singer, B. S., Jiménez, N. C., and Ort, M. H.: 40Ar/39Ar chronostratigraphy of Altiplano-Puna volcanic complex ignimbrites reveals the development of a major magmatic province, Geol. Soc. Am. Bull., 123, 821-840, https://doi.org/10.1130/B30280.1, 2011.

Schindlbeck, J. C., Kutterolf, S., Freundt, A., Eisele, S., Wang, K.-L., and Frische, M.: Miocene to Holocene Marine Tephrostratigraphy Offshore Northern Central America and Southern Mexico: Pulsed Activity of Known Volcanic Complexes, Geochem. Geophys. Geosyst, 19, 4143-4173, https://doi.org/10.1029/2018GC007832, 2018.

Sepúlveda, F., González, E., and Tomlinson, A. J.: Geología y estructura del cuadrángulo Quebrada Arcas, región de Antofagasta, Chile, Servicio Nacional de Geología y Minería, Informe Registrado, IR-23-108, Santiago, Chile, 53 p., - Inscripción No. 2023-A-11832, 2023.

Sepúlveda, F., Vásquez, P., and Quezada, A.: Geochronological record of Cenozoic pyroclastic eruptive events, Coastal Range of northern Chile (20º - 21º S), International Geological Congress on the Southern Hemisphere GEOSUR 2013, Viña del Mar, Chile, 25-27 November 2013, 199, 2013.

Sepúlveda, F., Vásquez, P., and Quezada, A.: Cartas Patillos y Oficina Victoria, región de Tarapacá, Servicio Nacional de Geología y Minería, Carta Geológica de Chile, Serie Geología Básica, 167-168, Santiago, Chile, 107 p., ISSN:0717-7283 Inscripción No. 248.599, 2014.

Sulpizio, R., Zanchetta, G., Paterne, M., and Siani, G.: A review of tephrostratigraphy in central and southern Italy during the last 65 ka, Il Quaternario Italian Journal of Quaternary Sciences, 16, 91-108, -, 2003.

Tapia, C. A., Wilson, G. S., Ishman, S. E., Wilke, H. G., Wartho, J. A., Winter, D., and Martínez-Pardo, R.: An integrated sequence stratigraphic and chronostratigraphic analysis of the Pliocene, Tiburon Basin succession, Mejillones Peninsula, Chile, Global Planet. Change, 131, 124-147, https://doi.org/10.1016/j.gloplacha.2015.05.005, 2015.

Tomlinson, E. L., Arienzo, I., Civetta, L., Wulf, S., Smith, V. C., Hardiman, M., Lane, C. S., Carandente, A., Orsi, G., Rosi, M., Müller, W., and Menzies, M. A.: Geochemistry of the Phlegraean Fields (Italy) proximal sources for major Mediterranean tephras: Implications for the dispersal of Plinian and co-ignimbritic components of explosive eruptions, Geochim. Cosmochim. Acta, 93, 102-128, https://doi.org/10.1016/j.gca.2012.05.043, 2012.

Vakhrameeva, P., Koutsodendris, A., Wulf, S., Portnyagin, M., Appelt, O., Ludwig, T., Trieloff, M., and Pross, J.: Land-sea correlations in the Eastern Mediterranean region over the past c. 800 kyr based on macro- and cryptotephras from ODP Site 964 (Ionian Basin), Quat. Sci. Rev., 255, 106811, https://doi.org/10.1016/j.quascirev.2021.106811, 2021.

van Zalinge, M. E., Sparks, R. S. J., Cooper, F. J., and Condon, D. J.: Early Miocene large-volume ignimbrites of the Oxaya Formation, Central Andes, J. Geol. Soc., 173, 716-733, https://doi.org/10.1144/jgs2015-123, 2016.

Vásquez, P. and Sepúlveda, F. A.: Cartas Iquique y Pozo Almonte, región de Tarapacá, Servicio Nacional de Geología y Minería, Carta Geológica de Chile, Serie Geología Básica, 162-163, Santiago, Chile, 114 p., ISSN:0717-7283 Inscripción No. 235.688, 2013.

Vásquez, P., Sepúlveda, F., Quezada, A., Aguilef, S., Franco, C., and Blanco, N.: Cartas Guanillos del Norte y Salar de Llamara, regiones de Tarapacá y Antofagasta, Servicio Nacional de Geología y Minería, Carta Geológica de Chile, Carta Geológica de Chile, Serie Geología Básica, 195-196, Santiago, Chile, 93 p., ISSN:0717-7283 Inscripción No. 295.735, 2018.

Vineberg, S. O., Albert, P. G., McLean, D., Suzuki, T., Staff, R. A., Yamada, K., Kitaba, I., Kitagawa, J., Manning, C. J., Buckland, H. M., Jones, G., Nishizawa, F., Nakagawa, T., and Smith, V. C.: A detailed record of large explosive eruptions from Japan between ~120 and 50 ka preserved at Lake Suigetsu, Quat. Sci. Rev., 346, 109021, https://doi.org/10.1016/j.quascirev.2024.109021, 2024.

Wallace, K. L., Bursik, M. I., Kuehn, S., Kurbatov, A. V., Abbott, P., Bonadonna, C., Cashman, K., Davies, S. M., Jensen, B., Lane, C., Plunkett, G., Smith, V. C., Tomlinson, E., Thordarsson, T., and Walker, J. D.: Community established best practice recommendations for tephra studies—from collection through analysis, Sci. Data, 9, 447, https://doi.org/10.1038/s41597-022-01515-y, 2022.

Wennrich, V., Diederich-Leicher, J., Blanco-Arrué, B. N., Büttner, C., Buske, S., Sepulveda, E. C., Dunai, T., Feller, J., Galego, E., Hasberg, A., Leicher, N., López, D. A., Maldonado, J., Medialdea, A., Ninnemann, L., Perryman, R., Ríos-Contesse, J. C., Ritter, B., Scheidt, S., Vargas-Machuca, B., Yogeshwar, P., and Melles, M.: Unearthing the climate history of the Atacama Desert in northern Chile - deep drilling in two clay pans of the Coastal Cordillera, Sci. Drill., 34, 1-20, https://doi.org/10.5194/sd-34-1-2025, 2025.

Wilkinson, M. D., Dumontier, M., Aalbersberg, I. J., Appleton, G., Axton, M., Baak, A., Blomberg, N., Boiten, J.-W., da Silva Santos, L. B., Bourne, P. E., Bouwman, J., Brookes, A. J., Clark, T., Crosas, M., Dillo, I., Dumon, O., Edmunds, S., Evelo, C. T., Finkers, R., Gonzalez-Beltran, A., Gray, A. J. G., Groth, P., Goble, C., Grethe, J. S., Heringa, J., 't Hoen, P. A. C., Hooft, R., Kuhn, T., Kok, R., Kok, J., Lusher, S. J., Martone, M. E., Mons, A., Packer, A. L., Persson, B., Rocca-Serra, P., Roos, M., van Schaik, R., Sansone, S.-A., Schultes, E., Sengstag, T., Slater, T., Strawn, G., Swertz, M. A., Thompson, M., van der Lei, J., van Mulligen, E., Velterop, J., Waagmeester, A., Wittenburg, P., Wolstencroft, K., Zhao, J., and Mons, B.: The FAIR Guiding Principles for scientific data management and stewardship, Sci. Data, 3, 160018, https://doi.org/10.1038/sdata.2016.18, 2016.

Wörner, G., Mamani, M., and Blum-Oeste, M.: Magmatism in the Central Andes, Elements, 14, 237-244, https://doi.org/10.2138/gselements.14.4.237, 2018.

Wörner, G., Uhlig, D., Kohler, I., and Seyfried, H.: Evolution of the West Andean Escarpment at 18 S (N. Chile) during the last 25 Ma: uplift, erosion and collapse through time, Tectonophysics, 345, 183-198, https://doi.org/10.1016/S0040-1951(01)00212-8, 2002.

Wörner, G., Hammerschmidt, K., Henjes-Kunst, F., Lezaun, J., and Wilke, H.: Geochronology (40Ar/39Ar, K-Ar and He-exposure ages) of Cenozoic magmatic rocks from northern Chile (18-22 S): implications for magmatism and tectonic evolution of the central Andes, Rev. Geol. Chile, 27, 205-240, http://dx.doi.org/10.4067/S0716-02082000000200004, 2000.

Wulf, S., Kraml, M., Brauer, A., Keller, J., and Negendank, J. F. W.: Tephrochronology of the 100 ka lacustrine sediment record of Lago Grande di Monticchio (Southern Italy), Quat. Int., 122, 7-30, https://doi.org/10.1016/j.quaint.2004.01.028, 2004.